8-2003

Interpolation of Spatial Surfaces and Inferring Subsurface Transitions Using Electrical Conductivity

Robert Claborne Wilson
University of Tennessee - Knoxville

To the Graduate Council:

I am submitting herewith a thesis written by Robert Claborne Wilson entitled "Interpolation of Spatial Surfaces and Inferring Subsurface Transitions Using Electrical Conductivity." I have examined the final electronic copy of this thesis for form and content and recommend that it be accepted in partial fulfillment of the requirements for the degree of Master of Science, with a major in Biosystems Engineering Technology.

Robert S. Freeland, Major Professor

We have read this thesis and recommend its acceptance:

William E. Hart, John B. Wilkerson

Accepted for the Council:
Dixie L. Thompson

Vice Provost and Dean of the Graduate School

(Original signatures are on file with official student records.)

To the Graduate Council:

I am submitting herewith a thesis written by Robert Claborne Wilson entitled "Interpolation of Spatial Surfaces and Inferring Subsurface Transitions Using Electrical Conductivity." I have examined the final electronic copy of this thesis for form and content and recommend that it be accepted in partial fulfillment of the requirements for the degree of Master of Science, with a major in Biosystems Engineering Technology.

Robert S. Freeland
Major Professor

We have read this thesis
and recommend its acceptance:

William E. Hart

John B. Wilkerson

Accepted for the Council:

Anne Mayhew
Vice Provost and Dean of
Graduate Studies

(Original signatures are on file with official student records)

Interpolation of Spatial Surfaces and Inferring Subsurface Transitions Using Electrical Conductivity

A Thesis
Presented for the
Master of Science Degree
The University of Tennessee, Knoxville

Robert Claborne Wilson
August 2003

Dedication

This thesis is dedicated to my parents, Al and Debby Wilson, whose love, teaching, and support have guided me throughout my life. My appreciation is also expressed to my brother and sister and hopefully they will follow my lead in their educational successes. I also dedicate this thesis to my grandparents, Bob and Dorene Wert and Bud and Ella Wilson, who have encouraged me to excel in everything. I would also like to thank all my aunts, uncles, cousins, and friends who also encouraged me along the way. A sincere thank you is extended to my fiancée, Jessica Wilson, who would not let me give up on myself and whose love and devotion motivated me to finish. I would also like to thank Billy and Cindy Wilson for putting up with me on the weekends. Finally, I would like to thank God for giving me the ability, opportunity, and wisdom to pursue this degree.

Acknowledgements

The author would like to extend a special thank you to his major professor, Dr. Robert S. Freeland for his work, guidance, friendship, and input in this project. My appreciation is also extended to my committee members, Dr. William Hart and Dr. John Wilkerson for their help. I also thank the entire staff of the Biosystems Engineering and Environmental Science Department especially to Dr. John Ammons, Wesley Wright, Craig Wagoner, Henry Moody, and David Smith. I also thank the staff of Ames Plantation, and especially Mark Shiers for all of his help with my fieldwork. I would like to also thank Kevin Raley for describing the soil cores. I would particularly like to thank Melanie Hammond for her help in working up soil samples as well as serving as an editor of this document. I would also like to thank my fellow graduate students Will Pinson, Leroy Leonard, Emily Heinerich, and Elizabeth Williams for thesis support during my graduate career.

Abstract

Precision agriculture techniques are becoming more popular within the agriculture community as producers demand more return from an ever-decreasing amount of farmland. Increased environmental regulations are forcing farmers to reduce the input of fertilizers and agrochemicals on their crops. Innovative techniques in precision agriculture are enhancing traditional decision-making processes by offering multiple layers of data for a production field. It is difficult to determine the complex interactions that exist between factors affecting crop growth and the resultant management decisions. Strategies in precision agriculture attempt to modify customary practices in order to address the known variability of field conditions.

This case study evaluated some of the tools used to create spatial data maps and the relationship of those maps to various soil properties. Electromagnetic induction (EMI) and ground-penetrating radar (GPR) were used to examine the similarities and differences among spatial and temporal variations of soil water content, soil texture, and bulk soil electrical conductivity (EC_a) on a large research watershed in southwestern Tennessee. A protocol was developed that identifies spatial variations in EC_a patterns using geographical information system (GIS) maps. Soil cores were collected in areas of contrasting conductivity, which were identified by temporal EC_a maps. Repeated spatial measurements of EC_a, starting near field capacity and then progressing through the draining and drying process, supplied visually shifting patterns that correspond to dynamic soil moisture variations and subsurface morphology transitions.

After several seasons of acquiring data for other studies, it was noted that spatial EC_a patterns remained somewhat similar across data gathering events, shifting only in relative amplitude in relation to seasonal moisture levels. The overall EC_a patterns remained somewhat similar, regardless of field moisture conditions. Soil morphology was considered constant over the data acquisition period, with subsurface moisture variations being the major influence in differing EC_a maps during the same period. Follow-up soil coring analysis supported this assumption in this case study.

The interpolation of spatial EC_a maps creates a continuous surface that contains values at unsampled locations. Inverse distance weighted (IDW), ordinary kriging (OK), and radial basis function (RBF) were examined as potential interpolation algorithms. Data were gathered to investigate the influences of short-term conductivity shifts over the data collection period, as well as from travel route patterns and instrument orientation. Using root-mean-squared error (RMSE) to quantify the transformation accuracy of EC_a maps, a data collection method and an appropriate geostatistical model were determined for this particular case study. Analysis showed that a bidirectional travel path produced the highest quality map, as transformation inaccuracies were reduced when measurements were obtained in a manner by which all measurements were temporally contiguous. A skilled application of ordinary kriging (OK) also increased map quality in comparison to the inverse distance weighted (IDW) and radial basis function (RBF) interpolation methods. Due to variability in our data, we are not able to recommend the use of a single interpolation algorithm for all data gathering scenarios.

Table of Contents

List of Tables

Table Page

List of Figures

Figure Page

List of Abbreviations

ATV	All-Terrain Vehicle
cm	Centimeter(s)
DGPS	Differential Global Positioning System
DOQ	Digital Ortho Quad
EC_a	Bulk Soil Electrical Conductivity
EMI	Electromagnetic Induction
ESRI	Environmental Systems Research Institute, Inc.
GIF	Graphics Interchange Format
GIS	Geographical Information System
GPS	Global Positioning System
GPR	Ground-penetrating Radar
ha	Hectare
hr	Hour
IDW	Inverse Distance Weighted
m	Meter
min	Minute
MLRA	Major Land Resource Area
mS	milliSiemens
OK	Ordinary Kriging
r	Pearson correlation coefficient
R	Correlation coefficient
RBF	Radial Basis Function
RMSE	Root Mean-Square Error
TDR	Time Domain Reflectometry

Part I

General Introduction

Recent tightening of environmental and economic constraints in the field of agriculture has resulted in a need for more efficient management strategies. A successful farming operation requires a management system that maximizes crop production and minimizes the input of fertilizers and agrochemicals. Precision agriculture is a management system that addresses in-field variations to optimize inputs on a point-by-point basis. In the past, detailed knowledge of agricultural inputs has been prohibitively expensive to acquire; however, recent innovations in electronics, communications, and related software have removed previous hurdles (Jahns, 2000). Satellite communications, fast microprocessors, coupled with innovative software, mobile power sources, and the use of inexpensive sensors now enables producers to collect vast amounts of geo-referenced data in a short amount of time (Auernhamer, 1994). Most of the early work in precision agriculture focused on grid sampling to determine differences in soil nutrient contents for variable rate fertilizer applications (Wibawa *et al*., 1993). When remotely sensed crop data is coupled with precision agricultural tools, the over-and under-application of inputs can potentially be reduced. This strategy can improve profitability for the producer as well as reducing the threat of ground and surface water contamination from agrochemicals and fertilizers.

Most producers are slow to adopt new practices or to invest in cutting edge technology until they are certain their investment will improve yield, reduce risk, or decrease costs. An increased awareness of precision agriculture applications along with the technology driven markets of sensors and instrumentation have made this practice a cost-effective tool for producers to use in making important land management decisions.

The decisions that are made today can affect the environment immediately or generations from now.

Precision agriculture data consists of many different layers of information. Yield maps, soil surveys, fertility-grid sampling data, visible changes in soil appearance, and especially a producer's historical knowledge of crop growth in the area are valuable and widely available layers of data. Equally important, but more limited in availability, are aerial and satellite images, elevation maps, and soil conductivity maps. While each data layer has some value, the challenge lies in using each one properly. Assumptions that are made beyond the utility of the layer might be inaccurate (Lund *et al*., 1999). Yield maps are ideal representations of production quantities for a single year and a specific field. Yield maps do not give any indication as to why variability occurs. If yield maps are used to establish site-specific production goals, other data layers that confirm occurrence of certain features should accompany them.

The world is facing a decrease in the amount of farmland that is supporting an increased demand for food and fiber products. This demand creates a need for accurate soil maps, which are useful for making production and management decisions. The heterogeneous nature of soils has long been recognized, but there is a lack of tools to detect subtle shifts among soil properties (Johnson *et al*., 2001). Traditional soil evaluation techniques involve intrusive methods, which have a limited sampling density due to time and labor constraints. Soil core extraction is currently the most accurate method used to determine morphological properties, but due to the high spatial resolution requirements in precision agriculture applications, soil cores are prohibitively expensive

to acquire. There is a need to improve upon existing soil mapping techniques that would reduce the time and labor costs associated with acquiring the data.

Electrical conductivity measurements have been used to identify contrasting soil properties in the environmental and geological fields (Lund *et al*., 1999). Due to its relationship with soil physical properties, the measurement and mapping of bulk soil electrical conductivity (EC_a) has the potential to enhance soil resource mapping. In this case study an electromagnetic induction (EMI) meter was employed to measure EC_a nonintrusively. The instrument can measure EC_a without contacting the ground, thereby eliminating destruction of the underlying morphology. In many applications, a single soil property, such as moisture content, salinity, temperature, or particle size, is the primary factor controlling the conductivity. Thus, once the correlation between EC_a and this property is established, an EMI survey can be used to map this feature quickly and inexpensively (Jaynes, 1996).

The mobile EMI data collection system described by Freeland *et al*. (2002), can quickly and efficiently measure the conductivity of large agricultural fields. The previous method of manually collecting EC_a data was time consuming and labor intensive. Large fields could be surveyed, but the resolution of measurements was low. The mobile method of data collection gives the high-resolution data needed to facilitate soil mapping without taking additional time to setup a grid pattern.

A high resolution EC_a map can identify small inclusions that are not found on typical USDA order 2 soil maps, which allow for 1-ha inclusions. Areas of contrasting conductivity can be targeted for soil classification, and these areas are easily delineated

by an EC_a map. This will reduce the number of samples required to characterize a field or improve upon existing characterization by sampling typical and non-typical regions of the field. Field scale EC_a maps serve as a basis for developing soil-sampling strategies, which accurately reflect spatial variation within the field.

Temporal EC_a data were collected over a two-day period in a large agricultural field to direct our soil coring analysis. The areas of the field with the sharpest change over the shortest distance were targeted for analysis of soil moisture and physical properties. Two 40-m transects were identified and three cores were collected from each for analysis purposes.

Several different mathematical algorithms were used to create continuous raster-based EC_a maps. Three common interpolation algorithms were compared to determine the effects of each on map accuracy in the loessial soils of southwest Tennessee. The precise location and conductivity of each discrete sample point was recorded to create a conductivity map of the field.

Soil properties were also investigated to determine which influenced EC_a readings in a spatial and temporal manner. Soil moisture content, salinity, and EC_a measurements are not constant but dynamic values. Soil can take thousands of years to form, but certain properties are constantly changing due to environmental conditions.

Map inaccuracies often occur when continuous surfaces are created from point data. The manner in which points are interpolated, the spacing of points, and the distribution of samples all affect the resultant surface. In the last decade there has been an increased awareness of the importance of assessing the uncertainty of values at

unsampled locations and the need to incorporate this assessment in subsequent management decisions (Goovaerts, 2001). Conductivity maps needed to make effective management decisions are not obtained in a single season but over the course of several seasons. A single season map is like a snapshot in time that can change quickly. Multiple maps over several growing seasons give a much better representation of data trends and patterns. A producer that has data from several seasons will be able to make more informed decisions about crop inputs.

The sensor industry has produced low-cost instruments that meet the need for high-resolution spatial data in precision agriculture applications. Instruments that do not have to come into contact with the target, such as the EMI meter, as well as others that bring the sensor in direct contact with the soil or plant surface, can be carried or towed in the field. The towed instruments are more capable than carried ones for collecting data in large agricultural studies as indicated by the use of our mobile EMI survey method. The use of ground penetrating radar (GPR) in tandem with EC_a data can potentially produce continuous subsurface profiles without disturbing the soil. There must be some form of soil disturbance for ground truth purposes, but it is minimal in comparison to traditional methods. Both EMI and GPR are fast, inexpensive, and can provide continuous ground measurements. Research by Doolittle and Collins (1998) found that neither technique works well in all soil environments. Ground-penetrating radar works best in soils that are low in clay content and relatively dry, due to the radar signal being highly attenuated in wet soils. Electromagnetic induction has been successfully used in a variety of soil conditions to detect conductivity in salty, wet, and even high clay content soils.

As a result of this case study, a protocol was developed that uses geophysical tools in addition to traditional methods for comprehensive site analysis. Essential to such protocol, soil scientists and geophysical technicians are refining techniques to map large sites for rapid soil mapping. Included in this new technique is the collection of soil cores, for ground truthing, along with noninvasive EMI and GPR data. The final geographical information systems map from the survey protocol incorporates digital ortho quads (DOQ's) for background maps of the field and surrounding areas. The utility of the survey protocol should be proven at several different test sites before widespread use of the protocol is recommended.

The geophysical team conducts the EMI and GPR surveys, while the soil scientists collect and analyze the soil samples. This thesis will concentrate on EMI data collection protocols. See appendix for protocol and data acquisition technique specifics for GPR. The current survey protocol for EMI data collection is as follows:

1) Both teams of researchers identify a field to be surveyed. The field needs to be free of trees and power lines, which can influence the performance of the geophysical equipment.

2) Based on the size of the field, the geophysical team determines which method of data collection to use from previous research (Leonard, 2001).

3) A geophysical technician calibrates the EMI instrument near the survey site before data collection begins.

4) The geophysical team executes the initial EMI survey in the horizontal dipole mode, which gives a maximum exploration depth of 3 m. An additional survey in

the vertical dipole mode can be collected if deemed necessary. The vertical dipole mode allows a maximum exploration depth of 6 m. In addition to EC_a readings, global positioning systems (GPS) data were collected at each measurement location in the field.

5) A conductivity map is rapidly produced for in-field evaluation by both teams. The soil scientists decide where to take soil samples by examining the conductivity map(s). Ideally, there are multiple surveys from which to gather information since conditions can change quickly.

6) Once the soil coring sites are identified from conductivity maps, the points are entered into a handheld GPS unit for navigation purposes. The soil scientists collect and describe the samples in 10 cm increments to a depth of 2.5 m. The samples are analyzed for particle size and nutrient and moisture content.

The combination of geophysical instruments in conjunction with minimal or no soil coring can potentially make these soil mapping applications more attractive to producers who would otherwise not use the technology. The number of small farms in the country is decreasing, and producers are looking for any advantage that will increase profit while reducing inputs of fertilizer and agrochemicals. Large farms will utilize this technology more readily than small farms because of their larger budgets and greater potential for profit. Once EC_a maps are created for a field, soil management zones can be delineated.

Today successful producers must stay informed on new and emerging technology while relying on traditional methods at the same time. However, techniques associated with precision agriculture are being widely incorporated into other sciences. While more research is conducted, the cost of sensors and instruments will continue to drop while at the same time quality and accuracy will continue to increase. This will ideally simplify these procedures to the point that minimal training is required to use and understand them. There are certainly many more applications that are relevant to precision agriculture than we will discuss in this case study. The boundaries of precision agriculture are far reaching and are limited only to a person's imagination as to what products to use and how to use them.

References

Auernhammer, H. 1994. Global positioning systems in agriculture. *Comput. Electron. Agric*. 11: 1.

Doolittle, J.A., and M.E. Collins. 1998. A comparison of EM induction and GPR methods in areas of karst. *Geoderma* 85 (1): 83-102.

Freeland, R.S., R.E. Yoder, J.T. Ammons, and L.L. Leonard. 2002. Mobilized surveying of soil electrical conductivity using electromagnetic induction. *Applied Engineering in Agriculture* 18(1): 121-26.

Goovaerts, P. 2001. Geostatistical modeling of uncertainty in soil science. *Geoderma* 103 (1-2):3-26.

Jahns, G. 2000. Navigating agricultural field machinery [introduction]. *Comput. Electron. Agric*. 25 (1-2): 1-2.

Jaynes, D. 1996. Improved soil mapping techniques using electromagnetic induction surveys. In P.C. Robert, R.H. Rust, and W.E. Larson, editors. *Proceedings of the Third International Conference on Precision Agriculture*; 1996 June 23-26; Minneapolis, MN. Madison, WI: ASA, CSSA, SSSA. p 170-79.

Johnson, K.J., J.W. Doran, H.R. Duke, B.J. Wienhold, K.M. Eskridge, and J.F. Shanahan. 2001. Field-scale electrical conductivity mapping for delineating soil condition. *Soil Sci. Soc. Am. J*. 65(6): 1829-1837.

Leonard, L.L. 2001. Mobile field systems for rapid subsurface data acquisition using electromagnetic induction and ground penetrating radar. Master's Thesis, University Of Tennessee.

Lund, E.D., C.D. Christy, and P.E. Drummond. 1999. Applying soil electrical conductivity technology to precision agriculture. In P.C. Robert, R.H. Rust, and W.E. Larson, editors. *Proceedings of the Fourth International Conference on Precision Agriculture*; 1998 July 19-22; St. Paul, MN. Madison, WI: ASA, CSSA, SSSA. p 1089-1100.

Wibawa, W.D., D.L. Dludlu, L.J. Swenson, D.G. Hopkins, and W.C. Dahnke. 1993. Variable fertilizer application based on yield goal, soil fertility, and soil map unit. *J. Prod. Agric*. 6 (2): 255-261.

Part II

Inferring Subsurface Morphology from Transient Soil Moisture Patterns Using Electrical Conductivity

Introduction

Our long-term research program involves developing survey protocols to identify areas that exhibit rapid horizontal movement of subsurface moisture, as this is a precursor of offsite agrochemical migration. Using electromagnetic induction (EMI) technology, we are developing survey protocols to identify areas that exhibit rapid horizontal movement of subsurface moisture. Our premise is that by identifying susceptible regions within agricultural production fields of rapid off-site water movement, producers can then implement best management practices that help reduce the risk of offsite contamination.

Since 1991, our multidisciplinary water quality research team has conducted a watershed-scale research effort to study the offsite movement of waterborne agrochemicals in southwestern Tennessee. The research fields are representative of thousands of hectares of soils that formed in the loess-covered Tertiary-aged Claiborne and Wilcox geologic formations (Hardeman, 1966). The research watershed resides within Major Land Resource Area 134 (MLRA 134—Southern Mississippi Valley Silty Uplands), which follows beside the Mississippi River from southern Illinois into northern Louisiana (fig. 2.1)(all figures located in appendix). The fields are essentially flat, with less than 0.5% slope, and have a parent material sequence of loess-alluvium-Tertiary sand (Ultic Hapludalfs). A distinct soil horizon interface commonly occurs between the loess and the underlying and sandier alluvium that forms an abrupt textural discontinuity. In places, the interface becomes a mixing zone. This textural discontinuity creates transient saturated conditions that can greatly influence vertical and lateral moisture movement.

Since dry soil is a poor electrical conductor that becomes an increasingly better conductor with increased moisture content, the value of EC_a (bulk electrical conductivity) is a "relative" indicator of its volumetric soil water content. Within a given homogeneous block of soil, a wetter region will have higher EC_a values than a drier region. However, a single EC_a value is a poor direct predictor of absolute soil moisture, especially across fields that have variations of soil texture (*e.g.*, sand being a poorer conductor than clay under similar field moisture conditions), soluble salt concentrations, and temperature (Freeland, 1989). Due to the very apparent influence of moisture on soil conductivity, individuals have attempted to determine soil moisture directly from soil resistance measurements. However, soil moisture-sensing methods, such as TDR (time domain reflectometry) and neutron moisture probes are more reliable than resistive methods due to influences of temperature and salinity on soil conductivity.

Comparison of EMI technologies to the neutron moisture probe as the standard reference produced favorable results with a multiple coefficient of determination (R^2) between 0.58 and 0.64 (Sheets and Hendrickx, 1995). Kachanoski *et al.* (1988) compared spatial variations in soil properties with bulk, surface, and solution phase electrical conductivity. They found in soils with low dissolved electrolyte that EC_a, independent of a wide range in texture, explained 96% of the spatial variation in soil water content. Jaynes *et al.* (1995) used EMI to correlate EC_a readings to the K_d (soil-partitioning coefficient). After calibration, the maps proved to be useful in determining leaching potential of herbicide applications in specific areas of the field. Another study by

Kachanoski *et al.* (1990) correlated EC_a readings to soil water storage and found that 50-60% of the variability in soil water content was explained by variations in EC_a.

Doolittle *et al.* (1994) used EC_a measurement as an estimator of claypan depth in an area of Mexico soils in central Missouri, finding a high correlation to the response of an EM38 meter. Eigenberg *et al.* (2002) linked a mobile EM38 induction system with global positioning system (GPS) to identify the dynamic changes in available soil N, as affected by animal manure and fertilizer. Corwin *et al.* (1993) used a mobile EM38 linked with GPS to investigate salinity levels within irrigated fields to forage yield and chemical analysis. The mobile system helped to establish a soil sampling scheme to characterize soil property spatial variability. Sudduth *et al.* (2001) also developed a mobile GPS-linked EM38 system, and investigated the accuracy issues in the collection of soil EC_a data. Although concerned with instrument drift, the sensitivity to speed and height was observed to be relatively minor. They noted that whole-field maps of EC_a from multiple surveys were similar but not identical.

Freeland *et al.* (2002) implemented a mobile survey method for nonintrusively measuring the depth-weighted average of EC_a (fig. 2.2). Using GIS (geographic information system), this procedure produced spatial EC_a maps by linking synchronized time stamps embedded within data streams of both a DGPS (differential global positioning system) receiver and an EC_a data logger, which is an option of the data logger software for conducting mobile surveys. Inman *et al.* (2002) employed this system on the research watersheds to gather EC_a data for comparison with laboratory analysis of pedon sample cores. They found percent sand to have a strong positive linear relationship with EC_a, while no other soil physical property produced a statistically significant relationship.

After several seasons of acquiring field data, Inman *et al.* (2002) noted that spatial EC_a patterns for a field remained somewhat similar across data gathering events, shifting in relative amplitude along with seasonal moisture levels. The overall EC_a pattern remained somewhat similar on a relative low-to-high scale, regardless of overall field moisture levels. From this basic observation, we formed a hypothesis that soil physical properties not changing with time caused the spatial pattern similarity. Furthermore, we assumed that any temporal pattern dissimilarity was a function of soil moisture, since it was the only known rapidly changing variable that affected soil EC_a.

Objectives

The objectives of this project were to:

1. Develop and evaluate a survey method for generating temporal EC_a maps,
2. Evaluate the soil properties that may be responsible for dissimilar spatial EC_a patterns in the loess-alluvium-Tertiary sand region, and
3. Develop numerical methods to identify areas of the field with similar and dissimilar EC_a variation patterns.

Materials and Methods

Survey equipment used in this project included: 1) two non-intrusive soil EC_a meters, a Geonics, Inc. EM-31 and EM-38 (probing at approximately 6 m and 1.5 m in the horizontal dipole orientation), 2) a non-metallic carrier for transporting the deep-probing EM-31 EC_a meter pulled by all-terrain utility vehicle (fig. 2.2), and 3) GIS and DGPS for spatial mapping and real-time positioning (fig. 2.3).

The EM31-MK2 and EM38-RT meters (Geonics Ltd., Mississauga, Ontario, Canada) detect near-surface geological variations, groundwater contaminants, or any

subsurface features that affect noticeable changes in ground conductivity (Geonics, 1995). A patented electromagnetic inductive technique allows measurements without ground contact. The instruments have a manufacturer-rated sensing depth of approximately 6 m (EM31-MK2) and 1.5 m (EM38-RT), recording EC_a values in milliSiemens per meter (mS/m). If rotated 90º along its longitudinal axis, both meters measure EC_a to one-half depth. The instruments work by energizing a transmitter coil, while a receiver coil detects the induced currents in the earth caused by time-varying magnetic fields. A secondary magnetic field is generated by the currents that the receiver coil senses along with the primary field. The ratio of secondary-to-primary magnetic fields is linearly proportional to terrain EC_a, which makes it possible to create a direct reading (McNeill, 1980).

Freeland *et al.* (2002) described an instrument carriage that transports the EM31-MK2 conductivity meter during surveys. An all-terrain vehicle (ATV) tows the carriage, which cradles the EMI instrument during data collection (fig. 2.2). To minimize ambient conductivity interference, the carriage consists of non-metallic components, primarily structural fiberglass. Evaluation testing has ensured that electrical noise and metal components from the ATV did not appreciably affect EMI readings (Freeland *et al.*, 2002).

An AgGPS 132™ (Trimble Navigation Limited, Sunnydale, CA, USA) supplied real-time, differentially corrected data with sub-meter accuracy. The DGPS antenna was mounted directly over the EMI console (fig. 2.2). A GIS package (ArcView 8.2, Environmental Systems Research Institute, Inc., Redlands, CA) allowed the importation of raw geographical location data, linked via time stamp to EC_a values, in order to

generate spatial EC_a maps. The interpolation method employed for creating the maps from the discrete data points was ordinary kriging using a spherical semivariogram with a variable search radius of twelve nearest points. The grid density was one square meter with a sample density of 0.06 points per square meter

Because the potential for rapid change in moisture content is much higher closer to field capacity (USDA, 1997), surveys began following an extended rainfall when soil moisture levels neared field capacity, and as soon as surface conditions permitted cross-field travel (fig. 2.4). From these surveys, two linear transects were established for soil core extraction by noting examining and dissimilar patterns using empirical calculations "RATE" and "CAPACITY" (fig 2.5).

Numerical Methods

The data are four-dimensional (*i.e*., latitude, longitude, EC_a, and time). An animated graphics interchange format (GIF) allowed displaying of these sequential events in movie format, producing a repeating time-sequence animation of the EC_a survey events. To depict the data statically, we reduced the data into three dimensions by forming two empirical variables that were functions of EC_a and time. We defined the first variable "RATE" as the slope of the best-fit line through the time vs. temporal EC_a data, thus having the units of *conductivity / time*. A second variable "CAPACITY" as the area beneath this curve (fig. 2.5), having the units of *conductivity x time*. Each of the spatial EC_a surveys constituted a GIS layer, with two additional calculated layers containing the spatial plots of "RATE" and "CAPACITY". We made the initial assumptions that finer texture profiles would probably have higher "CAPACITY" and lesser "RATE" values,

while coarser texture profiles would exhibit lower “CAPACITY” and steeper “RATE” values.

Soil Properties

Located near Grand Junction, Tennessee on the Ames Plantation (N 35^{o} 8' 11", W 89^{o} 13' 41"), the survey site resides on an upland position with an average site elevation of 156 m above mean sea level (fig. 2.1). Measured loess thickness ranges from 55-175 cm and measured alluvium thickness ranges from 100-235 cm. The USDA Field Survey (1964) mapped the entire survey site as either a Memphis or Loring silt loam.

For a groundtruth of the EMI data, two linear transects were established (fig. 2.5), each passing through regions that continually exhibited sharply differing EC_a temporal patterns that were derived as “RATE” and “CAPACITY”. For core sampling, we focused on regions having shifts of relatively high-to-low EC_a levels that occurred over a short distance, thereby signifying a possible morphological boundary or transition zone.

During the drier field conditions of the subsequent survey, a truck-mounted drill rig (CME-45B) extracted soil cores along the two linear transects to a 4-m depth, one each from high, medium, and low EC_a regions. The drill rig employed a 7.62-cm hollow-stem auger with extendable 76.2-cm long Shelby tubes. Each tube remained in the ground for 3 min. to ensure retrieval of an intact sample. Immediately after coring, a reciprocating saw sliced each tube into three equal lengths. The segments were transported back to the lab and extruded from the Shelby tubes in an effort to reconstruct the soil profile. Mineralogy, drainage, moisture content, horizons by depth, and other significant features were described by a soil scientist using standard laboratory procedures. Particle size was determined using the hydrometer method (Day, 1965).

To examine the influence of feature depth and method of measurement along the transects, subsequent EMI measurements (mobile EM31, manual EM31, and manual EM38) were taken the following summer before core sampling, once the preceding day (May 15, 2002) and once immediately prior to soil core extraction (May 16, 2002) during ground truth sampling. We defined "Manual" measurements as when the EMI instruments are hand carried during data acquisition, as opposed to "Mobile" where a vehicle tows the instrument mounted upon a carriage.

Results and Discussion

Survey Methodology

Traversing the entire site using the mobile method for complete field coverage (7.5 ha) required approximately 1.5 h (fig. 2.3), while equipment setup, calibration, and data transfer required an additional 1.5 h. This time lag prevented continuous data collection between surveys. The surface conditions and area of the research site permitted complete field survey coverage twice daily, once in the morning and once in the afternoon. Surveying continued for two days until rainfall resumed, allowing four time-sequential surveys (fig. 2.6).

Spatial plots of "CAPACTIY" and "RATE" for the entire field are presented in figs. 2.7 and 2.8. Regions of low "CAPACITY" values illustrate probable high sand content areas, whereas regions of higher "CAPACTIY" regions depict probable higher clay content areas (fig. 2.7). A small number of distinct regions of the field had positive "RATE" values, pointing to an increase in EC_a with time, a possible indicator of drainage accumulation areas (fig 2.8).

The series of time-elapsed EC_a maps suggest a temporal drying/draining pattern across the field (fig. 2.6). Table 2.1 (all tables located in addendix)contains statistics summarizing all of the point data for the entire site, where mean and maximum conductivities indicate a downward trend in EC_a measurements with time, supporting the known occurrence of a field drying/draining event. Temperature measurements taken at a depth of 12 cm were similar, which indicates little or no effect on changes in EC_a. Ambient air temperature and relative humidity variations did not have an apparent affect in the overall trend in EC_a. The change in salinity of the soils within this non-irrigated field was not a significant factor during the short time period over which data collection occurred, as these soils are nonsaline.

Along both transects, soil coring in high EC_a regions located a higher content clay layer beginning at the loess-alluvium interface, requiring noticeably extra force by the drill rig to continue coring. Extracting the core from the high EC_a regions was difficult. In contrast, very little force was required to core in the low EC_a regions. Coring effort at the medium EC_a sites required coring forces between these two extremes.

As expected, all measured soil properties to the coring depth correlate well with EM-31 measurements, with percent sand content being the highest, followed by moisture and clay percentages (Table 2.2). However, the EM-38 correlation values were much lower compared to soil physical properties (Table 2.2), an indicator of its limited depth of penetration over the extent of the sample coring depth. Because the two meters did not correlate well, this indicated that subsurface influences on conductivity were occurring beyond the range of the EM-38. The exact probing depth of neither meter was known,

only that the readings were depth averages, with near-surface features having a greater influence on the readings than deeper features.

Mobile and manual EM-31 measurements had a Pearson correlation coefficient (r) of .89 to .98 over the two-day period (Table 2.3), indicating that the two survey methods were similar. As predicted, high Multiple Pearson correlation coefficients (r) were found when comparing clay and sand percentages (Table 2.4) with "CAPACITY" (area beneath the curve with units of EC_a x time) and "RATE" (slope of best-fit line with units of EC_a/time) values.

Figure 2.9 illustrates the physical properties by depth of the six cores extracted from the two transects. Cores sampled from the two high EC_a regions had thicker loess layers layer than cores sampled from lower EC_a regions. In addition, the percent clay in the alluvium layer was higher. Low EC_a region core samples exhibited higher sand percentages rising nearer to the surface.

Summary and Conclusions

A method of generating temporal EC_a maps was developed by collecting multiple maps over a short interval following field capacity, and applying the method to a field in southwestern Tennessee. We identified two distinct areas of the field that had significant EC_a variations over a short distance by viewing spatial maps.

To better depict the data graphically, we reduced the data into three dimensions by forming two empirical variables, RATE and CAPACITY, which were functions of both EC_a and time. Targeting areas of abrupt transitions, we identified two transects that exhibited significant EC_a shifts over short distances. We collected EC_a data with EM-31 and EM-38 (deep and shallow probing) instruments before and after extracting soil cores

in relative high, medium, and low EC_a areas of the transect. Corresponding soil properties and EC_a measurements showed statistically similar trends for this site, with the EM-31 readings better typifying the depth extent of subsurface feature variability at this site. However, on shallow feature sites, the EM-38 may provide better results.

For this site, we subjectively inferred that soil morphology was the major factor for EC_a pattern similarity across time following field capacity. As the field drained/dried, the pattern dissimilarity was inferred as due to the moisture variation. Whereas a single EC_a measurement may be a poor direct indicator of soil moisture or morphology in itself, temporal measurements of EC_a followed by spatial analysis of pattern similarities and dissimilarities hold promise as one tool in subsurface investigations of soil morphology and moisture migration.

For example, regions exhibiting greater RATE and lower CAPACITY values exhibited a faster change in conductivity and less overall conductivity, which for this site correlated to thinner loess and shallower sands. These soil physical characteristics typify faster moisture rate of change and less moisture holding capacity; thus, one may wish to investigate restricting chemical application within these regions if susceptible water bodies are nearby.

References

Corwin, D.L., S.R. Kaffka, J.W. Hopmans, Y. Mori, J.W. van Groenigen, C. van Kessel, S.M. Lesch, J.D. Oster. 2003. Assessment and field-sale mapping of soil quality properties of a saline-sodic soil. Geoderma. 114(3-4): 231-259.

Day, P.R. 1965. Particle Fractionation and Particle-Size Analysis. In: Methods of Soil Analysis. Part I., C. A. Black (ed), Soil Sci. Soc. Amer. Madison,WI

Doolittle, J.A., K.A. Sudduth, N.R. Kitchen, and S.J. Indorante. 1994. Estimating depths to claypans using electromagnetic induction methods. J. Soil and Water Cons. 49(6) 572-575.

Eigenberg, R.A., J.W. Doran, J.A. Nienaber, R.B. Ferguson, and B.L. Woodbury. 2002. Electrical conductivity monitoring of soil condition and available N with animal manure and a crop cover. Agriculture, Ecosystems and Environment. 88(2): 183-193

Freeland, R. S. 1989. Review of soil moisture sensing methods using soil electrical conductivity. Transactions of the ASAE. 32(6):2190-2194.

Freeland, R. S., R.E. Yoder, J.T. Ammons, and L.L. Leonard. 2002. Mobilized surveying of soil conductivity using electromagnetic induction. Applied Engineering in Agriculture. 18(1) 121-126.

Geonics, Ltd. October 1995. EM31-MK2 Operating Manual. Mississauga, Ontario, Canada.

Hardeman, W.D. 1966. Geologic Map of Tennessee (West Sheet). State of Tennessee Department of Conservation, Division of Geology, Nashville, TN.

Inman, D.J., R.S. Freeland, J.T. Ammons, and R.E. Yoder. 2002. Soil investigations using electromagnetic induction and ground-penetrating radar in southwest Tennessee. Soil Sci. Soc. Am. J. 66(1): 206-211.

Jaynes, D.B., J.M. Novak, T.B. Moorman, and C.A. Cambardella. 1995. Estimating herbicide partition coefficients from electromagnetic induction measurements. J. Environ. Qual. 24:36-41.

Kachanoski, R.G., E.G. Gregorich, and I.J. Van Wesenbeek. 1988. Estimating spatial variations of soil water content using noncontacting electromagnetic inductive methods. Can. J. Soil Sci. 68:715-722.

Kachanoski, R.G., E. De Jong, and I.J. Van Wesesbeeck. 1990. Field scale patterns of soil water storage from non-contacting measurements of bulk electrical conductivity. Can. J. Soil Sci. 70:537-541.

McNeill, J.D. 1980. Electromagnetic terrain conductivity measurement at low induction numbers. Tech. Note TN-6. Geonics Ltd., Mississauga, Ontario, Canada

Sheets, K.R. and J.M.H. Hendrickx. 1995. Noninvasive soil water content measurement using electromagnetic induction. Water Resour. Res. 31(10):2401-2409.

Sudduth, K.A., S.T. Drummond, and N.R. Kitchen. 2001. Accuracy issues in electromagnetic induction sensing of soil electrical conductivity for precision agriculture. Computers and Electronics in Agriculture. 31(3):239-264.

USDA, Natural Resources Conservation Service. 1997. National Engineering Handbook (NEH), Part 652.0202, Irrigation Guide. Page 2-4.

USDA Field Survey, Soil Conservation Service. 1964. Soil Survey of Fayette County, Tennessee. U.S. Gov. Printing Office, Washington, D.C.

Appendix

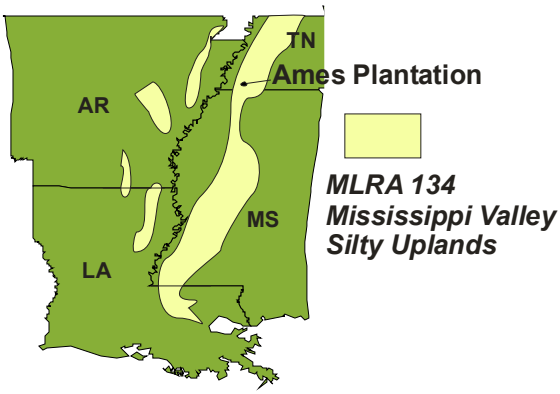

Figure 2.1-- Position of Ames Plantation within MLRA 134.

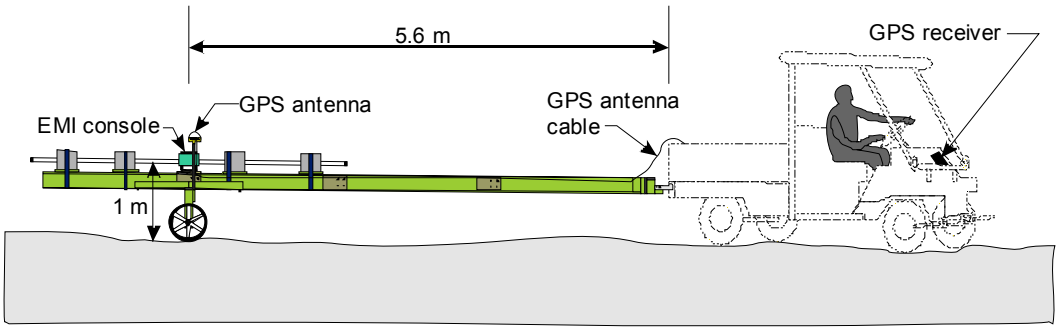

Figure 2.2-- EMI carriage and DGPS components (Freeland *et al.*, 2002).

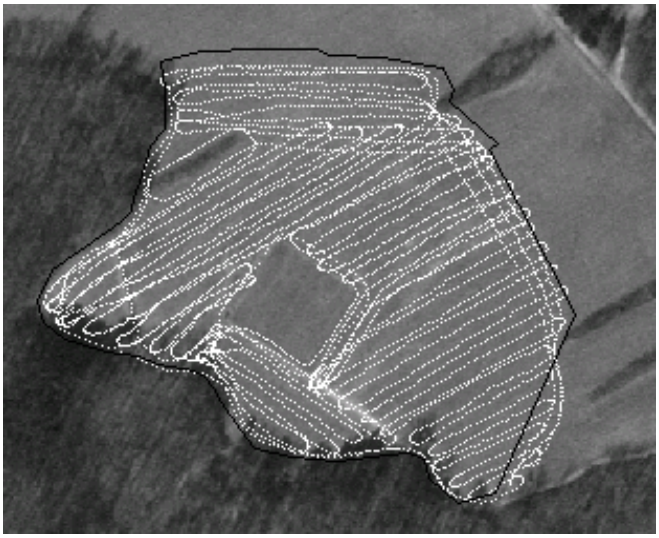

Figure 2.3-- Travel track of a mobile EM31 survey depicting sample points.

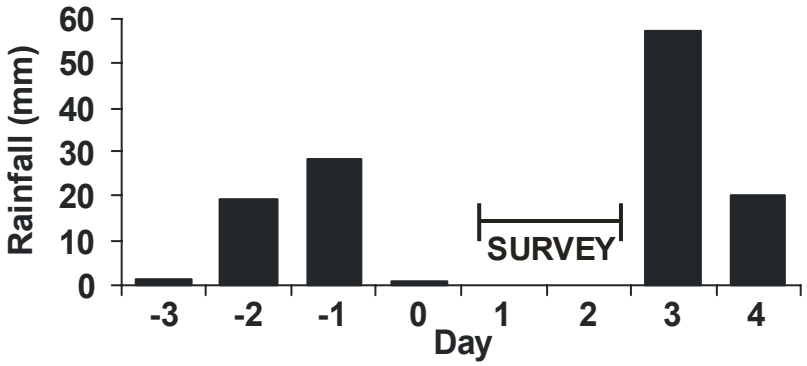

Figure 2.4-- Surveys taken during respite in rainfall (December 10, 2001 and December 11, 2001).

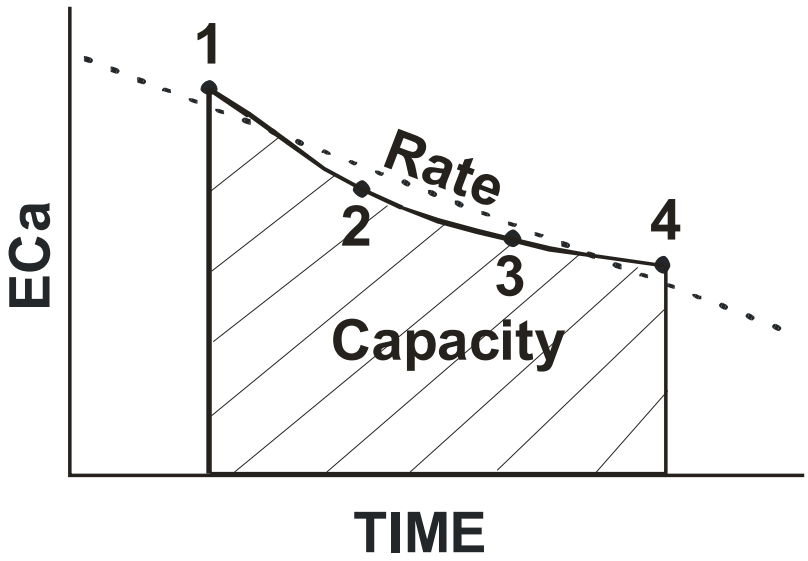

Figure 2.5-- Illustration of two assumptions in selecting two survey transects from four temporal conductivity measurements.

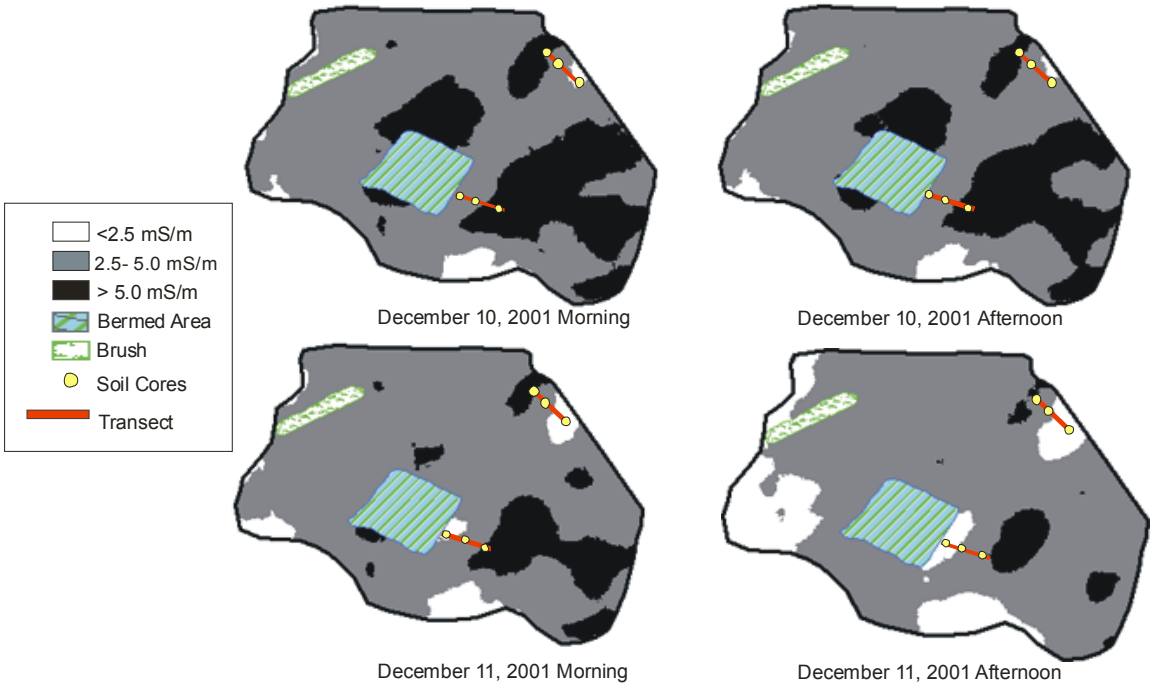

Figure 2.6-- Conductivity patterns over a 36-h period using mobile EM31.

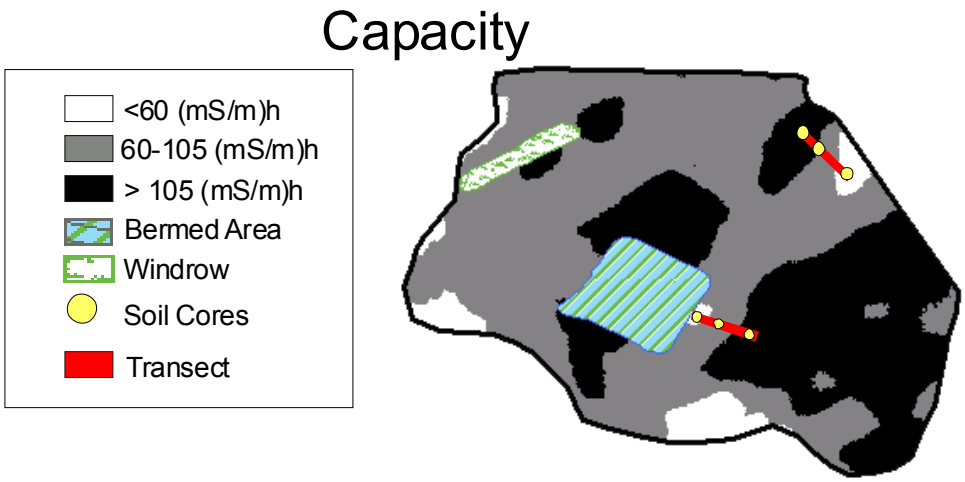

Figure 2.7-- Capacity pattern (area beneath the curve) of four surveys illustrating high (black) to low (white) overall conductivity levels.

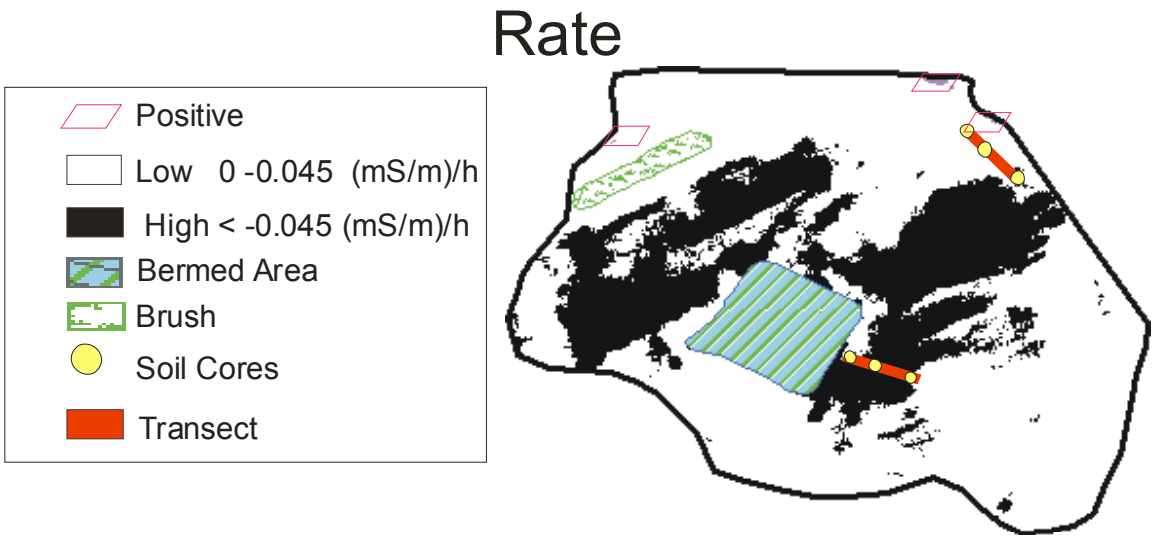

Figure 2.8-- Rate pattern (slope of best-fit line) of four surveys illustrating high (black) to low (white) rate of conductivity decrease. Positive sites had increase in conductivity with time, an indicator of moisture gain.

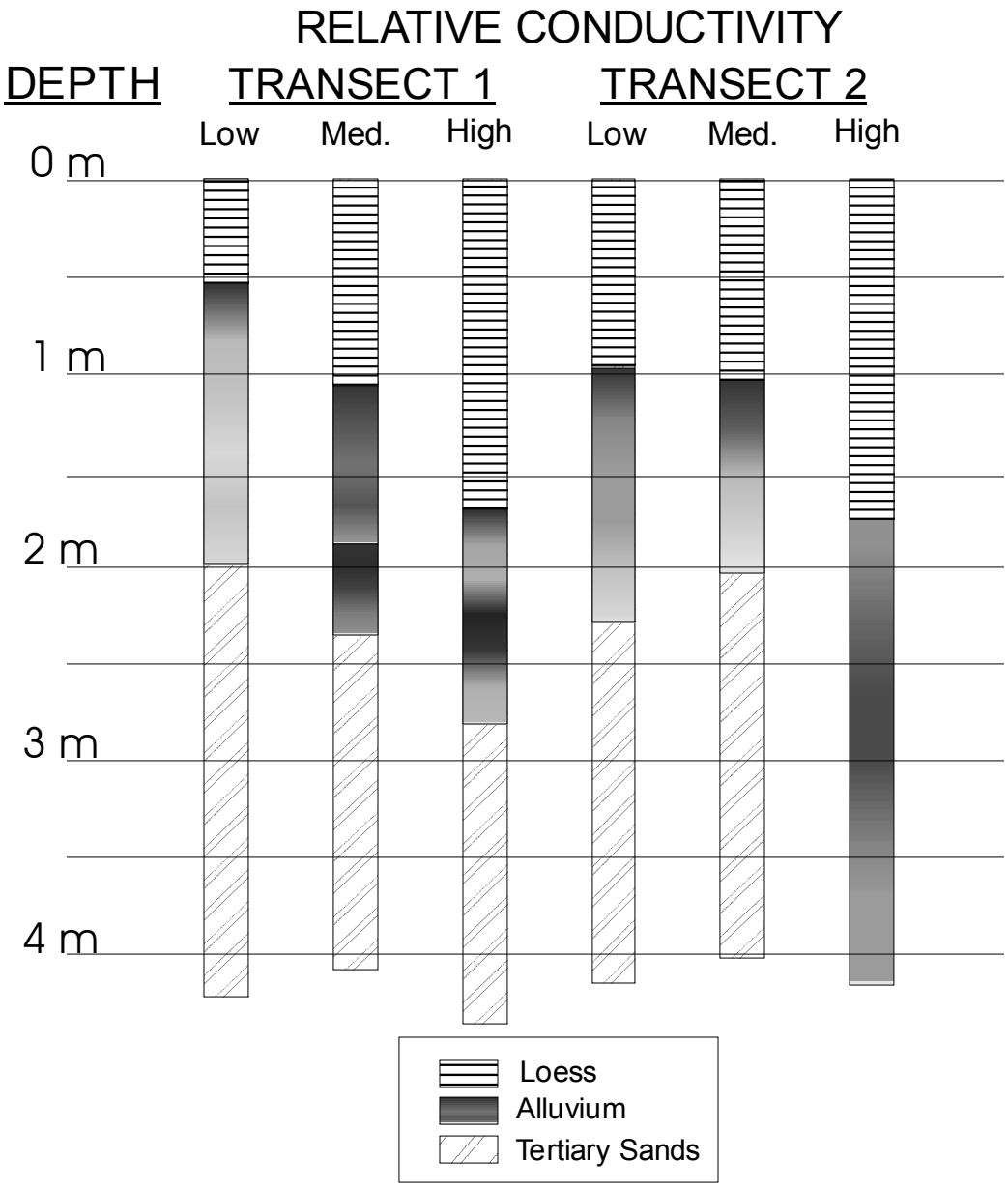

Figure 2.9-- Loess, alluvium, and tertiary sands parent material by depth, with darker shaded regions of alluvium layer representing higher clay content.

Table 2.1--Temporal variations for entire field survey

		Mobile EM 31 Conductivity (mS/m)				Temp. (°C)
		Mean	Min.	Max.	Std Dev.	Mean
12/10/01	Morning	4.100	0.386	7.269	1.108	9.7
	Afternoon	4.070	0.550	7.082	1.057	10.8
12/11/01	Morning	3.876	0.112	6.688	1.034	9.6
	Afternoon	3.190	0.024	6.299	1.091	10.6

Table 2.2--Pearson correlation coefficient (r) of six core locations (May 15, 2002 and May 16, 2002)

	Manual EM31 (EC_a)		Mobile EM31 (EC_a)		Manual EM38 (EC_a)	
	5/15/02	5/16/02	5/15/02	5/16/02	5/15/02	5/16/02
Clay† (%)	*0.86	0.74	0.72	0.64	0.44	0.41
Sand† (%)	**-0.98	**-0.97	**-0.94	*-0.91	-0.72	-0.77
Bulk density†	0.16	0.28	0.44	0.49	-0.21	0.20
Moisture† (% d.b.)	0.76	*0.87	*0.82	*0.90	0.68	0.85

*Correlation is significant at the 0.05 level (2-tailed)
**Correlation is significant at the 0.01 level (2-tailed)
†Entire 4-m soil core, with effective depth of 1.5 m and 6 m for EM38 and EM31, respectively

Table 2.3--Pearson correlation coefficient (r) of EC_a data obtained over two transects using three methods (May 15, 2002 and May 16, 2002)

		Manual EM31		Mobile EM31		Manual EM38	
		5/15/02	5/16/02	5/15/02	5/16/02	5/15/02	5/16/02
Manual EM31	5/15/02	1	**0.96	**0.95	*0.89	0.65	0.70
	5/16/02	**0.96	1	**0.98	**0.97	0.72	*0.86
Mobile EM31	5/15/02	**0.95	**0.98	1	**0.98	0.56	0.76
	5/16/02	*0.89	**0.97	**0.98	1	0.61	*0.85
Manual EM38	5/15/02	0.65	0.72	0.56	0.61	1	*0.85
	5/16/02	0.70	*0.86	0.76	*0.85	*0.85	1

*Correlation is significant at the 0.05 level (2-tailed)
**Correlation is significant at the 0.01 level (2-tailed)

Table 2.4--Correlation coefficient (R) of soil physical properties and assumptions illustrated by fig. 6

	"RATE"	"CAPACITY"	Combined
Clay (%)	0.76	0.83	0.89
Sand (%)	0.56	0.62	0.66
Moisture (d.b.)	0.20	0.24	0.30

Part III

Data Collection and Interpolation Techniques for Mapping Soil Bulk Electrical Conductivity

Introduction

Our research involves mapping subsurface moisture pathways within the loessial-over-alluvium soils of southwest Tennessee. Identifying these pathways help to target possible agrochemical migration patterns. Towards this goal, spatial maps of bulk soil electrical conductivity (EC_a) can nonintrusively highlight major shifts in soil morphology and soil moisture regime patterns. Repeated short-interval surveys have revealed that positional EC_a measurements are dynamic, and are multidimensional in regard to instrument orientation. We have observed that mapping accuracies vary depending upon the interpolation method and/or model employed, and from the route taken across the field while gathering data.

We employ an EM31-MK2 (Geonics Ltd., Mississauga, Ontario, Canada) conductivity meter to nonintrusively measure EC_a to an optimal depth of 6 m. Whenever it is desired to probe shallower, the instrument can be rotated 90^o along its longitudinal axis to take measurements at approximately half this depth (Geonics, 1995). McNeill (1980) gives a complete description of the function and theory behind the EM31-MK2 and its operation. Subsurface transitions are detected by first detecting a change in EC_a while moving across the field. Pivoting the instrument horizontally about a point over a transition zone and observing maximum to minimum readings gives a sense of the boundary orientation.

Measurements of EC_a across large fields are typically obtained with some form of mobile transport, such as a towed, cart-mounted conductivity meter described by Freeland *et al.* (2002) (Fig. 3.1a) (all figures located in the appendices). Data are sampled

at closely spaced, geo-referenced points within the field. From this data set, Geographical Information Systems (GIS) software is used to create continuous-surface EC_a maps using one of several interpolation models. As this mobile protocol is typically more time extensive and covers more acreage than a pedestrian survey where the instrument is hand held (Fig. 3.1b), considerations of temporal effects and instrument orientation are essential.

During post processing, spatially interpolating discrete EC_a data can also produce pattern inconsistencies. A discrete field point above a subsurface transition area may conceivably yield a full range of EC_a values. Varying readings for a discrete field point may be related to the instrument's height above the point, calibration drift, and the time-varying soil moisture content and ambient conditions (Sudduth *et al*., 2001). These observations of mapping inconsistencies has led to an examination of the available geostatistical interpolation models and methods to determine which one produced EC_a spatial maps with the "best" transformation accuracy, where accuracy is defined as the predictable agreement between meter measurements (true or erroneous) and the resulting spatially interpolated surface. Furthermore, field tests focused on a variety of driving pattern scenarios, as this affected both sample time and instrument orientation.

Literature Review

Englund (1990) performed a study where identical spatial data sets were given to twelve geostatistical investigators. Each investigator was asked to independently analyze the same data set and create spatial interpretations. Results varied considerably, in part due to the vast number of models, methods, and options that are available for producing spatial maps.

Goovaerts (2001) noted that no one interpolation model works well in all cases, but rather there exists a "toolbox of algorithms" from which to select appropriate methods. The selection of a particular interpolation model depends on characteristics of the data set as well as the study objectives. Individual models can contain numerous user-defined settings, methods, and variables that influence mapping transformation accuracy. With larger data sets, some are more processing-intensive and require more user-selected model parameters than other simpler, less robust models.

A review of the literature showed many interpolation model studies for the natural sciences. For example, researchers have studied the relationships between ordinary kriging (OK) and inverse distance weighted (IDW) for mapping soil nitrate (NO^{-3}) and organic matter content for variable-rate fertilizer applications in corn production (*Zea mays L.*) on Midwest soils (Gotway *et al.*, 1996). They found that OK provided reasonably accurate results in all cases. They also found that model accuracy was dependent upon the soil parameter being mapped. Burgess and Webster (1980a, 1980b) used punctual and block kriging to estimate soil properties for small and large blocks of land. They concluded that block kriging was more appropriate than punctual kriging in estimating average values over large areas. They also found kriging to be especially pertinent to physical properties associated with water in the soil. Bishop and McBratney (2001) evaluated the performance of multiple linear regression, OK, and Kriging with External Drift (KED) for mapping Cation Exchange Capacity (CEC) using the secondary variables of yield, EC_a, elevation, and satellite images. They suggested that KED, with the use of secondary information such as EC_a, could more accurately predict the CEC than could OK. Isaaks and Srivastava (1989) compared OK, IDW, and triangulation on

several clustered data sets and found that OK produced the lowest prediction error in their applications. Niemann *et al.* (2001) compared real surface data to the radial basis function (RBF)-derivative Completely Regularized Spline (CRS) and fractal interpolation methods on topographic data in simulated river networks. The CRS method was viewed as the smooth interpolator, in this case, while the fractal method was a rough interpolator. They tested the ability of each method to estimate unobserved elevations, slopes, and curvatures as well as to simulate their distribution. The CRS interpolation produced better estimates of slope than the fractal method. They concluded that the CRS method was a good compliment to existing interpolation methods used in simulating river networks.

As suggested above, each application is often a function of human prerogative and individual analytical skill. In fact, multiple approaches may be taken to explore different aspects of the data set. This study focused on three interpolation models found in ArcMap 8.2 Geostatistical Analyst (ESRI, Inc., Redlands, CA): IDW, OK, and RBF. However, the concepts used to evaluate the model results presented herein may be applied to other interpolation models and software platforms.

Common Interpolation Models

The IDW model creates a surface from measured points based on their similarity and distance. Weights are assigned to control points during interpolation, such that the influence of one point relative to one another decreases with distance from the calculated point. As the power increases, the closer the value of the calculated point is to the nearest observed point (Isaaks and Srivastava, 1989). Inverse distance weighted gives reasonable results for many types of data as well as being easy to use and calculate. When using IDW, the choice of weighting function is difficult if there is a non-uniform spatial

distribution of data points. Also, the occurrences of maximum and minimum values occur only within the range of measured data. This model is more likely to produce "bull's eyes" around data points.

Due to its robustness and effectiveness, kriging has become almost synonymous with spatial interpolation among laypersons. However, the flexibility provided by certain kriging models may require extensive analyst decisions. Kriging derives its weights from variation patterns expressed within a semivariogram, whereby an optimal model (*e.g.*, circular, exponential, logarithmic, Gaussian, *etc*.) is fitted by the analyst for calculating unmeasured points. The semivariogram illustrates the spatial correlation among measured and unmeasured points as a function of separation distance and directional angle within a search window. One method of kriging is OK, a flexible form of kriging where there are few assumptions, but as such can be less powerful than other kriging methods.

Radial basis functions are flexible, and can handle regularly spaced or scattered data points. There are many forms of RBF, but this study focused on the CRS function. Pollution concentrations, elevation points, water table heights, and other gently varying surfaces are well suited for RBF interpolations (Johnston *et al.*, 2001). The weight of a CRS point is defined by the third derivative in a curve minimization expression. The overall curvature of the surface is reduced and interpolated data are forced through a specified number of data points. Radial basis functions are simple to compute, requiring only the solution of linear equations (Hickernell and Hon, 1999).

Mapping Transformation Accuracy

The ultimate goal in generating spatial maps is supplying an accurate surface representation as provided by the measured control points. A concept known as "jack-

knifing", or cross validation, removes each control point one at a time. Its replacement value is then calculated using the model. The difference determined between the actual and predicted values, repeated for all control points within the data set, forms an indicator of mapping transformation accuracy. Various validation indices can be used as a measure of prediction quality, the most common of which are the root-mean-squared error (RMSE) and mean error (Bishop and McBratney, 2001).

Objectives

Our field experience suggested that three sources of mapping inconsistencies or transformation inaccuracies can occur due to (1) temporal soil conductivity shifts and instrument calibration drift over an extended data collection period, (2) instrument orientation due to driving pattern, and (3) from the application of a selected interpolation model itself. The objectives of this case study for our field site were to:

1. Determine if EC_a data collection driving patterns have an influence on the mapping consistency of interpolated surface EC_a maps,
2. Investigate any short-term temporal effects upon EC_a mapping consistency, and
3. Evaluate common interpolation models (IDW, OK, RBF) as to the impact of each model on transformation accuracy when mapping EC_a.

Materials and Methods

Bulk soil electrical conductivity data were gathered using a mobile system (fig. 3.1a) that allowed automated measurements over large acreages without a pre-established survey grid (Freeland *et al.*, 2002). Using differential global positioning system (DGPS), geospatial data were merged with EC_a data using synchronized time stamps. Resultant data were imported into ArcView 8.2 (ESRI, Inc., Redlands, CA) for spatial mapping and

interpolation purposes. A large concrete pad was installed in a shaded area that is adjacent to the site for calibration and monitoring instrument drift. The in-phase reading of the EM31 was re-zeroed over this pad immediately prior to each survey.

Using this survey method, three studies were conducted to determine the effect of data collection procedures on map transformation accuracy. The first study took place on a small 0.4-ha plot with instrument orientation as the variable. Data were collected in three different instrument orientations (fig. 3.2). A bidirectional pattern involved collecting data in both opposing directions. Unidirectional data were extracted from the bidirectional data set, copying transect data that were traversed in only one direction, approximately northeast-to-southwest (N-S) and then southwest-to-northeast (S-N). Thus, the two unidirectional data sets are subsets of the bidirectional data set. Finally, a separate perpendicular pattern followed that consisted of driving in four directions, which required orthogonal repositioning after each subsequent pass.

The second study involved comparing non-continuous temporal data to a bidirectional survey on a 7.5-ha field (fig. 3.3). After an initial bidirectional survey, boundary passes encircling the field were driven that did not in all instances follow the orientation of the original bidirectional pattern. Thus, an instrument reorientation and a time delay in these measurements were introduced. The boundary passes were similar to headlands that are subsequently planted in the turn rows at the edge of a field. Boundary passes help to fully encompass the survey by smoothing the erratic end-of-row turning points in the bidirectional survey, and also to establish the outer boundary coordinate trace for the survey map.

The final study was in a nearby field of similar size to the second study, where both planned and non-planned driving patterns were evaluated (fig.3.4). First, a non-planned driving pattern was driven by an operator using personal choice. The operator had no prior knowledge of the test results from the previous two studies. The operator was instructed to canvas the entire field. A follow-up survey, the planned survey, was where the operator relied on information gained from the previous study that predicted the optimal driving pattern.

Each of the data sets from the three studies was evaluated using a standardized methodology, whereby similar parameters were used when possible for the models. A single sector spherical search neighborhood that incorporated ten surrounding data points determined the value at unsampled locations. The OK interpolation parameters included using a spherical semivariogram to estimate the weighting factor. A power of two was used to determine weighting values in the IDW interpolation. The RBF interpolation used a CRS function to calculate unknown values.

Results and Discussion

The results are presented in terms of "best" transformation accuracy, where accuracy is defined as the predictable agreement between EC_a measurements (true or erroneous) and the resulting spatially interpolated surface. The parameter RMSE was selected as the transformation accuracy indicator, as it is available for OK, IDW, and RBF. There is no assessment of prediction errors for IDW and RBF in ArcMap 8.2 Geostatistical Analyst (ESRI, Inc., Redlands, CA).

Figure 3.5 presents the RMSE values for the small plot driving pattern tests illustrating influences due to data collection methods as well as interpolation models.

Small differences were observed between instrument orientations (N-S, S-N) in the unidirectional data, as they also had the largest RMSE. The bidirectional data produced the lowest RMSE in the driving pattern tests, and by observation, it is also the most time-efficient driving pattern. The lower RMSE may also be due to the denser sampling rate of the bidirectional pattern as compared to the unidirectional pattern, and the latter is a subset halved from the former (table 3.1) (all tables located in the appendices). The maps produced in the perpendicular survey had higher RMSE than the bidirectional survey. However, its RMSE was lower than the unidirectional orientations.

Figure 3.2 presents a visual interpretation of each method including data point sampling location and resultant interpolation map. The original point data values for each of the four maps are identical, but the three resultant maps from applying OK, IDW, and RBF models exhibit noticeable pattern differences.

The field scale boundary study encompassed a larger survey area, which included significantly more data points (tables 3.1 & 3.2). Interestingly, the RMSE values between the field scale study (fig. 3.6) and small plot study (fig. 3.5) were comparable, but the numbers of points gathered in the field scale survey were substantially higher. In this instance, the field scale survey produced the least RMSE with IDW interpolations, just slightly less than OK. Ordinary kriging using various semivariogram models (table 3.3) consistently produced an RMSE of approximately 0.2 across all data sets in regard to bidirectional, no boundary, and planned surveys.

Figure 3.3 highlights a small area of the larger field scale study that produced the "bull's-eye" pattern when using IDW as the interpolator. This pattern is evident where subsequent boundary passes intersect at a right angle the initial bidirectional survey

points over a transition zone. The same pattern was not visually apparent when using OK and RBF interpolation models.

The survey technique study determined that planned surveys produce lower RMSE maps than non-planned surveys. Figure 3.7 depicts lower RMSE values for the planned survey. Visual interpretation of the data (fig. 3.4) indicates little variability between the maps produced by each model. Differences are apparent between RMSE values as compared between each of the models (fig. 3.7). Ordinary kriging produced lower RMSE results in the planned survey, while IDW produced lower RMSE results in the non-planned survey.

Summary and Conclusions

This manuscript discusses the potential sources of errors when mapping discrete EC_a measurements. Three sources of mapping inconsistencies or transformation inaccuracies are from (1) temporal soil conductivity shifts and instrument calibration drift over an extended data collection period, (2) instrument orientation due to driving pattern, and (3) from the application of a selected interpolation model itself. Mapping transformation accuracy was evaluated by comparing RMSE values for each of the interpolation models as well as the different data collection methods. Selection of an optimal surveying scenario, including post processing, was based upon minimizing RMSE as the goal. Using RMSE to quantify the transformation accuracy of EC_a maps, a data collection method and an appropriate geostatistical model were determined for the loessial soils of West Tennessee. The results are presented in terms of "best" transformation accuracy, where accuracy is defined as the predictable agreement between EC_a measurements (true or erroneous) and the resulting interpolated surface.

For this study site, the data collection driving pattern was found to influence the mapping transformation accuracy of continuous surface EC_a maps, with an opposing bidirectional orientation of the instrument supplying the smaller RMSE. Analysis showed that a bidirectional travel path helped to lower RMSE, as transformation inaccuracies were reduced when measurements were obtained in a manner that limited the directional influence of the EM31 orientation passing over subsurface transitions. The OK model demonstrated a trend of having lower RMSE values as compared to IDW and RBF models. Data that were gathered both spatially and temporally contiguous yielded lower RMSE.

References

Bishop. T.F.A., and A.B. McBratney. 2001. A comparison of prediction methods for the creation of field-extent soil property maps. *Geoderma* 103 (1-2):149-160.

Burgess, T.M., and R. Webster. 1980a. Optimal interpolation and isarithmic mapping of soil properties. I the semi-variogram and punctual kriging. *J. Soil Sci.* 31:315-331.

Burgess, T.M., and R. Webster. 1980b. Optimal interpolation and isarithmic mapping of soil properties. II block kriging. *J. Soil Sci.* 31:333-341.

Englund, E.J. 1990. A variance of geostatisticians. *Mathematical Geology*, 22(4): 417-455.

Freeland, R. S., R.E. Yoder, J.T. Ammons, and L.L. Leonard. 2002. Mobilized surveying of soil conductivity using electromagnetic induction. *Applied Engineering in Agriculture* 18(1): 121-126.

Goovaerts, P. 2001. Geostatistical modeling of uncertainty in soil science. *Geoderma* 103 (1-2): 3-26.

Geonics, Ltd. 1995. EM31-MK2 operating manual. Mississauga, Ontario, Canada: Geonics, Ltd.

Gotway C.A., R.B. Ferguson, G.W. Hergert, and T.A. Peterson. 1996. Comparison of kriging and inverse-distance methods for mapping soil parameters. *Soil Sci. Soc. Am. J*. 60 (4):1237-1247.

Hickernell, F. J., and Y.C. Hon. 1999. Radial basis function approximations as smoothing splines. *Appl. Math. Comput.* 102 (1):1-24.

Isaaks, E.H., and R.H. Srivastava. 1989. *An Introduction to Applied Geostatistics*. New York: Oxford University Press Inc.

Johnston, K., J. M. Ver Hoef, K. Krivoruchko, and N. Lucas. 2001. *Using ArcGIS Geostatistical Analysis*. Redlands, CA: ESRI Press.

Niemann, J.D., R.L. Bras, D. Veneziano, and A. Rinaldo. 2001. Impacts of surface elevation on the growth and scaling properties of simulated river networks. *Geomorphology* 40 (1-2):37-55.

McNeill, J.D. 1980. Electromagnetic terrain conductivity measurement at low induction numbers. Technical Note TN-6. Mississauga, Ontario, Canada: Geonics, Ltd.

Sudduth, K.A., S.T. Drummond, and N.R. Kitchen. 2001. Accuracy issues in electromagnetic induction sensing of soil electrical conductivity for precision agriculture. *Computers and Electronics in Agriculture* 31(3):239-264.

Appendix

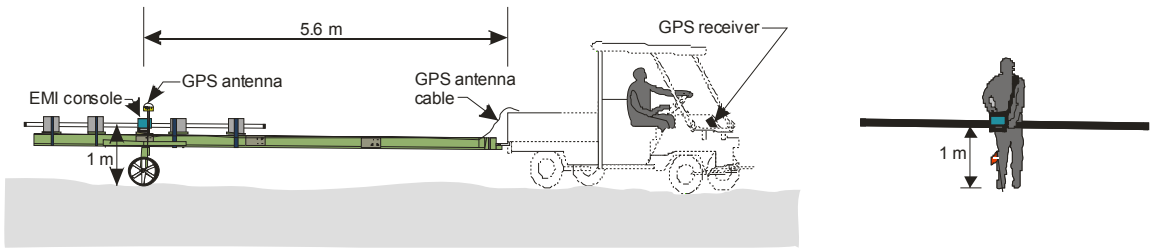

Figure 3.1-- (a) Mobile Survey System and GPS components: antenna positioned over EMI console, antenna cable suspended alongside carriage body, and GPS receiver (b) Conventional pedestrian survey

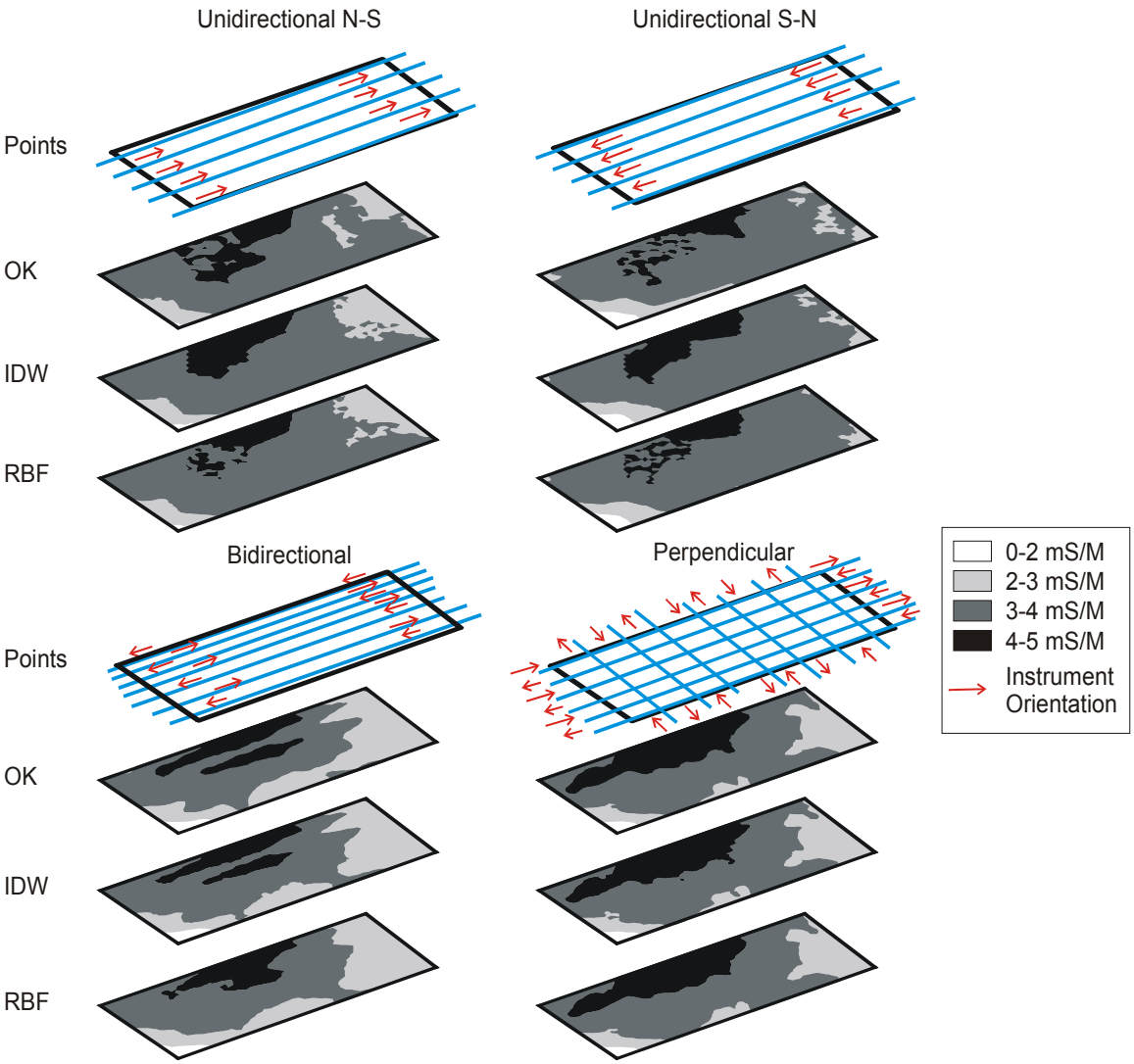

Figure 3.2-- Patterns and resultant interpolation maps from the small test plot (0.4 ha)

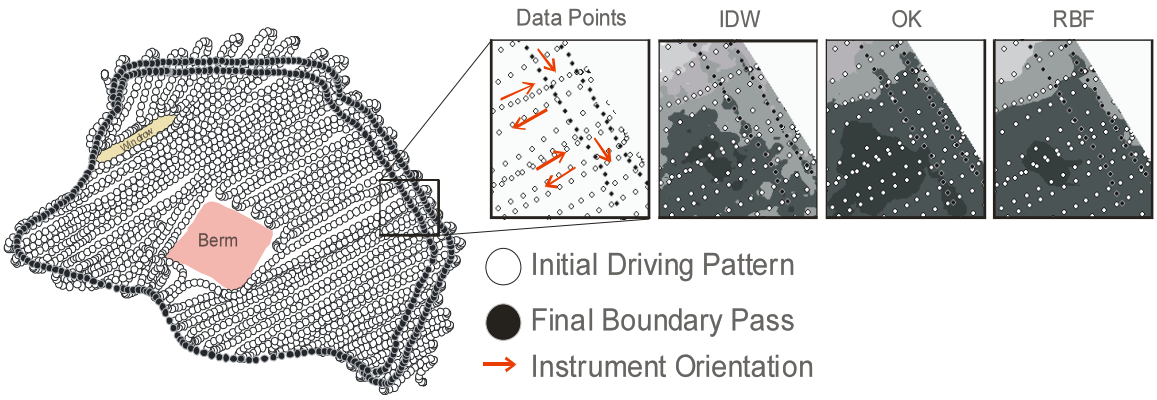

Figure 3.3-- Orientation of instrument and temporal shifts that produce a "bulls-eye" pattern in IDW interpolation

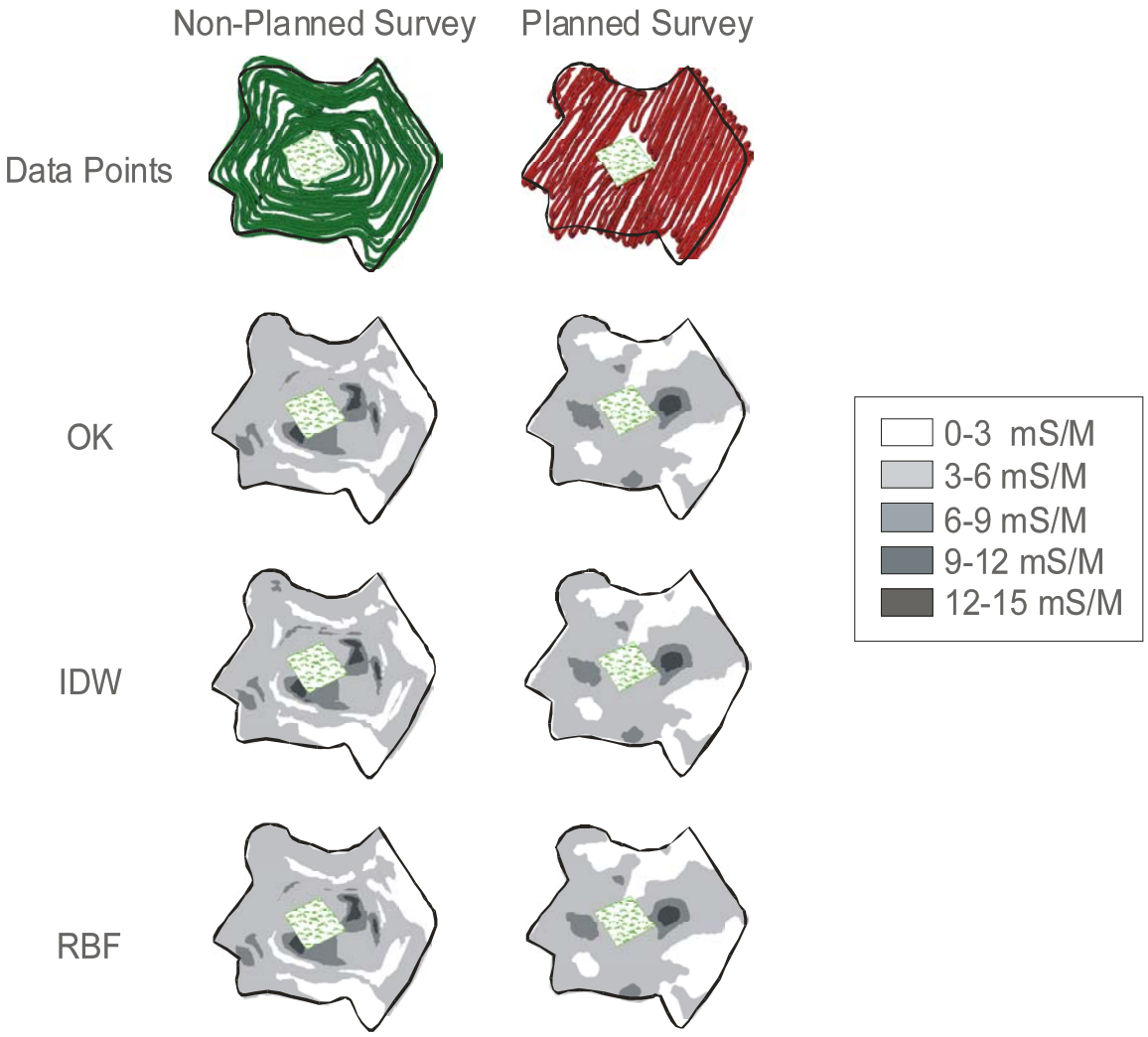

Figure 3.4-- Planned and non-planned survey maps with resultant interpolations for an adjacent field

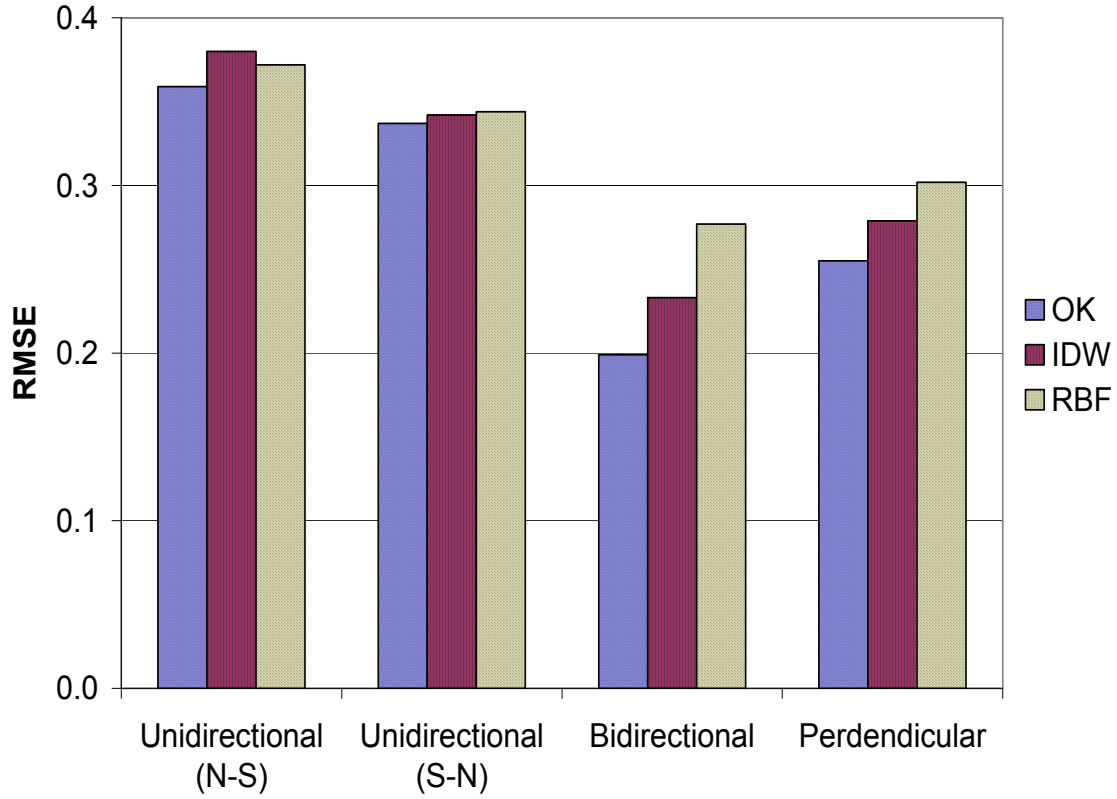

Figure 3.5-- Error comparisons of instrument orientation in small test plot (0.4 ha)

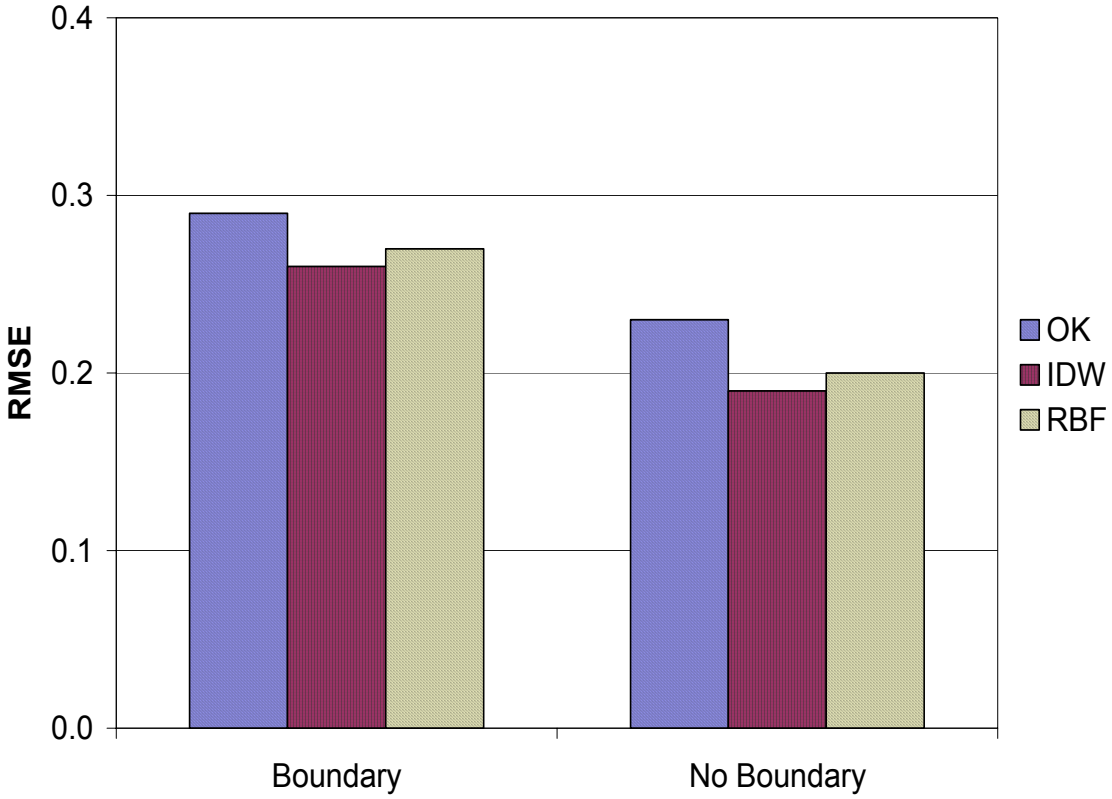

Figure 3.6-- Illustration of temporally and spatially contiguous and incontiguous sampling

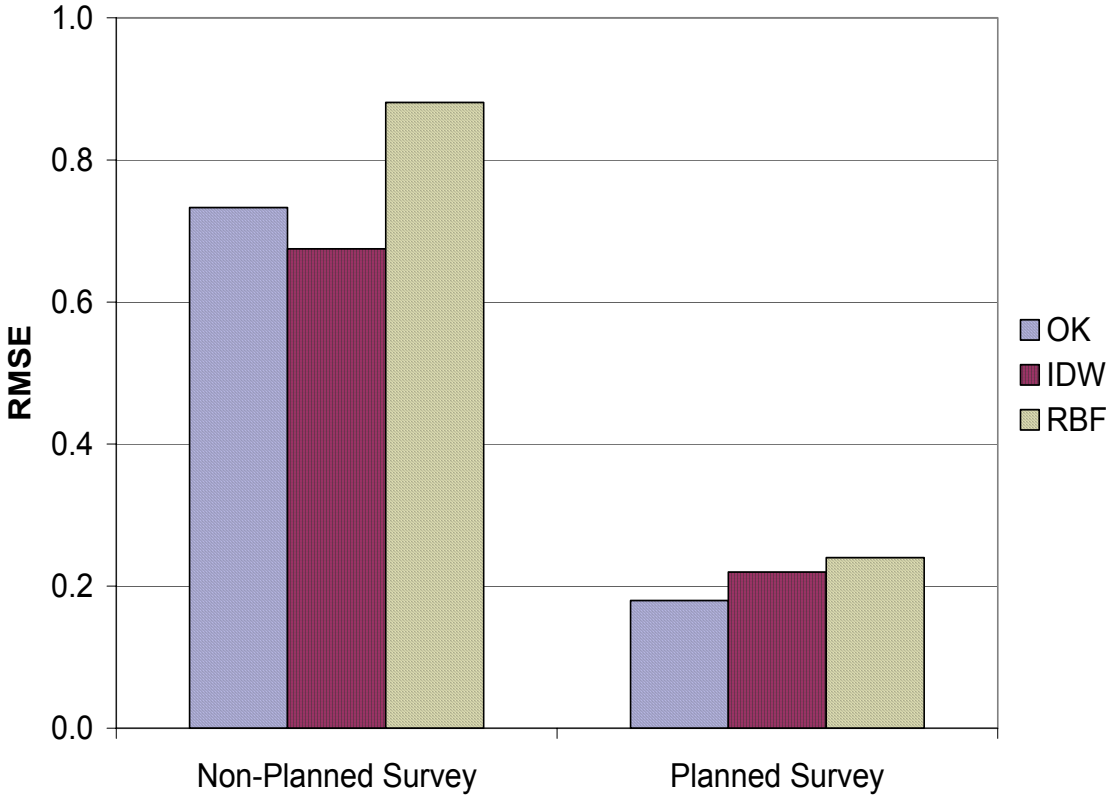

Figure 3.7-- Driving pattern error comparison

Table 3.1-- Test plot (0.4 ha) data points

Method	Data Points
Unidirectional (N-S)	381
Unidirectional (S-N)	349
Bidirectional	729
Perpendicular	766

Table 3.2-- Field scale (7.5 ha) data points

Method	Data Points
Boundary	4918
No Boundary	4558

Table 3.3-- RMSE values for selected semivariogram models using OK interpolation

Method	Circular	Spherical	Exponential	Gaussian	Stable
Unidirectional (N-S)	0.359	0.359	0.372	0.362	0.360
Unidirectional (S-N)	0.335	0.337	0.347	0.345	0.342
Bidirectional	0.199	0.199	0.200	0.223	0.217
Perpendicular	0.256	0.255	0.262	0.283	0.280
Boundary	0.284	0.283	0.272	0.292	0.292
No Boundary	0.228	0.227	0.212	0.238	0.238
Non-Planned	0.738	0.733	0.648	0.790	0.785
Planned	0.183	0.183	0.183	0.259	0.254

Part IV

Summary

The future of precision agriculture is promising, and the use of new technologies in conjunction with existing ones provides endless possibilities for products available to producers. There are many more potential uses for the technologies that were discussed in this case study. Although yield monitors, variable rate fertilizer applicators, and variable rate chemical applicators were not discussed, they are also important components of a successful precision agriculture program.

The use of temporal EC_a mapping techniques on spatial data has shown promise on the loessial soils of southwest Tennessee. Future studies on different soil formations in similar and alternate study areas will determine the efficacy of the proposed survey protocol. Incorporating some of the common mathematical interpolation algorithms into the protocol can aid in the creation of accurate spatial maps. This case study has demonstrated the correlation of EC_a maps to soil particle size and moisture content. The use of EC_a maps in precision agriculture applications goes further than simply directing soil core collection. Further testing will determine if different morphological features can be correlated to EC_a maps.

There is room for improvement in current mapping techniques, and the door is open to imaginations and new technologies for future research ideas. As we have seen in this case study, results can vary from survey to survey depending on field conditions. The amount of time over which data are collected is another avenue for future research.. An extended data collection period would be better for determining changes in temporal EC_a maps. A single survey is not a sound basis for making important management decisions. Multiple surveys should be conducted to obtain a more accurate representation of what is occurring in a field. A producer would ideally have multiple layers of data for the same

field in order to make management decisions concerning specific field treatments. This secondary data might include yield maps, soil maps, and aerial photographs that could be brought together in a geographical information system (GIS) format.

There are several interpolation algorithms available for creating continuous EC_a maps. This study only looked at three that are most common in commercial surface mapping software packages. There is an opportunity for development of new algorithms that improve upon the interpolation accuracy. Experimentation with different interpolation algorithm techniques can potentially yield more accurate maps. Combining the interpolation algorithms can possibly provide a more complete spatial analysis of the data because of unique functions within each method.

There are many settings within the algorithms themselves that can be fine-tuned in future research projects. In the OK interpolation, a spherical semivariogram was used to determine the weighting factor; but there are many other models from which to choose. Each semivariogram model could give slightly different results. In the IDW interpolation, we used a power of two; but any number can be used. The greater the number, the more influence there is from closer points. In the RBF interpolation, we used the CRS function to estimate values at unmeasured locations. The best algorithm is often determined by the configuration of the data set as well as the personal opinion of the scientist. Another determining factor in the selection of interpolation algorithms is the appearance of resultant maps. Smooth patterns are more visually appealing than ones that have a bull's-eye pattern.

The shape of the search neighborhood is influenced by the data and the surface you are trying to create. A directional influence of data points from wind or topography can impact map accuracy. In our case study, we assumed that there were no directional influences, so points were considered equally in all directions. A search neighborhood with directional influences would likely be in the shape of an ellipse and should be parallel to the influential feature. Options within the neighborhood's search area can restrict which data points within the shape are used, but the user can determine the minimum and maximum number of data points to consider. If the neighborhood is divided into sectors, each one will have the minimum and maximum values applied. We used a circular neighborhood with a single sector search, but multiple sector searches with different shapes are also options.

Alternate methods of data collection can also be implemented to determine the effect on map accuracy. The data collection methods that we employed in the small plot could be implemented on a large-scale basis in future research initiatives. Any number of data collection methods could be tested including a unidirectional travel path in a spiral pattern. The shape of the field can play a role in driving pattern tests, which would likely be the case with a unidirectional spiral pattern. A uniform distance between passes in any of the driving pattern tests could make a difference in map accuracy. Currently there is no means to determine uniformity between passes. The use of a parallel tracking device, such as a light bar, could provide a user defined distance between each pass. Different distances could be tested to see which one creates the most accurate map.

The primary focus of this case study was to investigate factors affecting the survey accuracy in the creation of spatial EC_a maps. The survey protocol that we outlined

also contains an extensive procedure for implementing GPR. There is potential for future research as a continuation of the current protocol by incorporating GPR in areas that have been extensively studied and mapped with the EMI. The protocol will likely require additional revisions after more study and further implementation of GPR technology. One area that is not addressed in the survey protocol that is of interest to the precision agriculture community is the use of remote sensing data. Images from satellites and aerial photographs will allow producers to quickly view an entire farm and make management decisions based on the remotely sensed data. Remote sensing is not a direct contact measurement; but by relating soil moisture and plant nutrient levels to field measurements, a producer can make inferences about large plots of land.

Using temporal EC_a maps to direct soil sampling can be a precursive study for GPR. The survey protocol suggested in the beginning of this case study is still in the early stages of testing. With more input the protocol can only be improved and implemented across varying landscapes. The collection of soil cores in our case study helped us to make inferences about similar areas within the field. Without some form of ground truth verification, it is nearly impossible to determine what you are initially looking at in a GPR survey. Once the soil morphological properties are related to the GPR scans, classification becomes easier

Some suggested improvements to the present method of EC_a data collection involve bringing the data logger closer to the operator in order for progress to be monitored during the survey. Presently, the data logger is inaccessible during the survey. If problems occur during the survey for any reason, the operator is unaware until completion of the survey, possibly ninety minutes later. A battery level indicator would

also prevent lost time during surveying due to power loss during data collection. If the operator could view the progression of data during the survey, both of these problems would be minimal.

The data from this case study indicate that a planned survey results in more accurate maps than non-planned surveys. The field scale studies typically involve more planning and time to investigate data accuracy issues. To reduce valuable time, a smaller plot was used to test data collection methods. On the loess/alluvium soils of southwest Tennessee, a mobile EC_a data collection method in a planned bidirectional survey with no boundary pass and either IDW or OK as the interpolation algorithm produces the most accurate results. Due to the variability of results obtained in this case study; we are unable to recommend the use of a single interpolation algorithm in all scenarios.

Appendix

Color	Horizon	Depth	Texture	Comments
10YR 4/4	Ap	0-5	SiL	MnO
7.5YR 4/4	Bt_1	5-15	SiL	MnO,+4% clay content
7.5YR 4/6	Bt_2	15-21	SiCL	MnO, clay films
7.5YR 4/4	$2Bt_3$	21-33	SiL	Few MnO, sand increase, clay films, stripped areas, redox features 28"
7.5YR 4/6	2Bt/C	33-42	L	Large E bodies, increased stripping, pref flow paths crotevena(few),concentrations >2%,clay films
7.5YR 4/6	2BC	42-48	L(SiL)	Less E bodies/stripping, few clay films, MnO
7.5YR 4/4	$2C_1$	48-54	SL	Few MnO, pockets of clay accumulation are common
7.5YR4/6	$2C_2$	54-57	L	Horizon may be a large pocket of clay accumulation within C
7.5YR 4/6	$2C_3$	57-67	SL	Fe common, Mn few, small pockets of clay accumulation few in #
7.5YR 4&5/6	2C4	67-78	LS	Fe common, Mn few
2.5YR 4/6	$3B't_1$	78-85	SCL	Fe and Mn common
(2.5)5YR4/6	$3B't_2$	85-95	SCL	Fe and Mn common, stripped E bodies
2.5YR 4/6	3BC	95-108	SL	Stripping/E bodies are more prominent, iron conc.
7.5YR 5/8	3C	$108\text{-}165^{+}$		Pred. sand pocketed with small areas of clay accumulations, dominant color is 7.5YR 5/8,areas of stripped material present throughout this horizon (7.5YR 8/2 & 8/3)

Transect 1-1

Parent material for this pedon is Loess over alluvium. Loess extended to a depth of 21 inches where a more recent alluvial deposit extended to a depth of 78 inches. The parent material present at 78 inches is also alluvium, but it is different in lithology than the 2 overlying parent materials. The layer that extends from 78 inches to 165 inches is marked by a developed paleosol at the upper boundary to 108 inches.

Described by Kevin Raley
Date:6-3-02

EMI DATA

Method	**Day one (mS/m)**	**Day two (mS/m)**
Manual (EM31)	3.5	1.8
Mobile (EM 31)	5.1	4.2
Manual (EM 38)	7.5	5.5

Lowest conductivity for the transect (expected and observed)

Color	Horizon	Depth	Texture	Comments
(7.5)10YR 4/6	Ap	0-4	SiL(high end)	Original surface may have been eroded. Roots are common, few crotovena
7.5YR 4/4	Bt_1	4-12	SiCL	Clay films, MnO common, striped areas
7.5YR 4/6	Bt_2	12-20	SiCL	Blind pores are common, few Fe conc., Mn conc. common, clay films abundant, strips
7.5YR 4/6	Bt/E	20-34	SiCL	A large volume of horizon is occupied by an E body(10YR 7/1),clay films abundant, blind pores common, Fe,Mn conc common
7.5YR 4/4	BC	34-43	SiL	Stripping, no reduced matrix, depletions(10YR 6/2) common within stripped matrix (10YR 7/1) Fe conc. common, blind pores, few clay films
7.5YR 4/4	$2Bw_1$	43-53	L(SiL)	Sand increases(horizon may be a mixing zone, Fe Mn conc. common, stripped areas, blind pores, few faint depleted areas visible
7.5YR 4/4 (3/4)	$2Bw_2$	53-60	SiL	Stripped areas, Fe Mn conc. common, may be part of mixed zone
7.5YR 5/4	$2Bw_3$	60-68	L	Striped areas, few Mn Fe conc., clay films present but not abundant or thick
5YR 5/6	2BC	68-73	SCL	Striped areas, few large macropores, large red clay bodies (5YR 5/8) blind pores common. Mn Fe conc. common
2.5YR 4/6	$3Bt_1$	73-81	CL	Mn Fe conc. common, large areas of preferential flow (stripped 7.5YR 7/1), few small macropores
2.5YR 4/6	$3Bt_2$	81-88	C	Large areas of stripped pref flow within clay matrix, Fe conc. common, macropores common
2.5YR 4/6	$3Bt_3$	88-94	SC	Lesser extent of stripping, Fe conc. common, mush less of volume is occupied by stripped areas, few blind pores
(5)2.5YR 4/6	$3C_1$	94-106	SL	Few blind pores, Mn conc. present, Fe conc. common
2.5YR 3/6	$4C_2$	106-135	SL & LS	Clay drops off (mainly sand), much deeper red
2.5YR 5/6	$4C_3$	$135\text{-}159^+$	LS	Few Mn conc.

Transect 1-2

Loess extends to 43 inches. At the boundary of the first lithologic discontinuity, there is evidence of restricted water movement as indicated by the presence of redox depletions in the BC horizon. The contrasting particle size between the loess/alluvium may be causing restriction of water flow. The parent material sequence is Loess over 2 recent (2,3) alluvial deposits over presumably tertiary alluvial deposits (4). The lower alluvium deposits were marked by the development of Paleosols at the upper boundaries (see colors).
Described by: Kevin Raley
Date: 6-4-02

EMI DATA

Method	**Day one (mS/m)**	**Day two (mS/m)**
Manual (EM31)	5.1	4.2
Mobile (EM 31)	6.57	5.88
Manual (EM 38)	9.3	7.7

Medium conductivity for the transect (expected and observed)

Color	Horizon	Depth	Texture	Comments
10YR 4/4	Ap	0-4	SiCL	Few Fe conc., roots common, few large macropores
7.5YR 5/6	BA	4-13	SiL	Few Mn Fe conc., roots common
7.5YR 4/6	Bt/E	13-22	SiCL	Large stripped E bodies (7.5YR 7/2), blind pores (few), Fe Mn conc. common
7.5YR 4/6	Bt_1	22-30	SiCL(SiL)	Few large macropores, few stripped areas(7.5YR 7/1), Fe and Mn conc. common, blind pores common, depletions common (7.5YR 6/2)
7.5YR 3/4	Bt_2	30-49	SiCL	Few stripped areas, Fe Mn conc. common, depletions (7.5 YR 6/2) common
7.5YR 4/6	Bt_3	49-63	SiL	Few striped areas, few Fe Mn conc., slight sand % increase
5YR 4/6	$2BC_1$	63-79	SiCl (CL)	7.5YR 6/2 depletions at lower bound, few large macropores, Fe conc. common, few stripped areas, blind pores common
2.5YR 4/6	$2Bt_1$	79-90	C	Fe conc. common, few stripped areas, Mn conc. common at lower bound 85-90 inches
2.5YR 5/6	$2Bt_2$	90-110	C	Fe, Mn conc. common, clay bands (2.5YR 4/6) are common within fine material (2.5YR 5/6) matrix
2.5YR 4/8	$3C_1$	110-122	SL	Few Mn Fe conc.
2.5YR 4/6	$3C_2$	122-132	SL	Few Mn conc.
5YR 5/6	$3C_3$	$132\text{-}170^+$	SL	Mn Fe conc. common

Transect 1-3

Loess extends to 63 inches. Bt_3 horizon may be a mixing zone between loess and alluvium as there was a slight increase in sand. Bt_1 and Bt_2 horizons contain depletions. Makes sense considering contrasting particle size class at the lithologic discontinuity. Dominant particle size class in 1st alluvial layer is clay (79-110 inches). This layer shows evidence of paleosol development evident by 5 YR and 2.5YR hues. The 2nd lithologic discontinuity occurs at 110 inches. These layers are presumably tertiary aged sand deposits. The majority of the areas of preferential flow are found in the losseial parent material.

Described by: Kevin Raley
Date: 6-5-02

EMI DATA

Method	**Day one (mS/m)**	**Day two (mS/m)**
Manual (EM31)	7.5	5.6
Mobile (EM 31)	8.4	7.7
Manual (EM 38)	10.3	8.4

Highest conductivity for the transect (expected and observed)

Color	Horizon	Depth	Texture	Comments
7.5YR 4/6	Ap	0-5	SiL (SiCL)	Roots common, few large macropores(root channels),
7.5YR 5/6	Bt_1	5-23	SiCL	Thick clay films, Mn Fe conc. common, few macropores at lower boundary
7.5YR 4/6	Bt_2	23-38	SiL(SiCL)	Mn conc. common, few small areas of stripping, clay films
7.5YR 4/4	$2BC_1$	38-50	L	Sand increase, large areas of stripping, Mn conc. common, Fe conc. few, few small macropores
7.5YR 4/4	$2BC_2$	50-65	SL	Few areas of stripping, few Fe conc.
7.5YR 4/4(5/4)	$2C_1$	65-77	SL	No real evidence of pedogenesis, few Mn conc.
7.5YR 5/4	$2C_2$	77-89	S	
2.5YR 4/6	$3C_3$	89-103	SCL(SL)	Paleosol interface, clay increases
2.5YR 4/8	$3C_4$	103-118	SCL(SL)	
2.5YR 4/8(5/8)	$3C_5$	118-133	SL(LS)	Few faint areas of stripping
2.5YR 5/8	$3C_6$	$133\text{-}162^+$	S	

Transect 2-4

Loess extended to 38 inches. No drainage impediment observed in this profile. Parent material sequence is loess over alluvium (2, 3). Both alluvial deposits showed little evidence of pedogenesis. There is evidence of paleosol development at the boundary of the second lithologic discontinuity (3). Colors switch sharply from 7.5YR 5/4 to 2.5YR hues at this boundary (rubification). Underlying horizons show little pedogenic modification.

Described by: Kevin Raley
Date: 6-5-02

EMI DATA

Method	**Day one (mS/m)**	**Day two (mS/m)**
Manual (EM31)	4.6	4.6
Mobile (EM 31)	4.7	5.3
Manual (EM 38)	7.0	8.0

Lowest conductivity for transect (expected and observed)

Color	Horizon	Depth	Texture	Comments
10YR 4/4	Ap	0-6	SiL	Few Fe conc., roots common
7.5YR 4/6	Bt1	6-18	SiCL	Mn conc. common, in lower portion of horizon, few small macropores (2mm)
7.5YR 4/6	Bt2	18-33	SiCL	Mn conc. common, Fe conc. common in lower portion, clay films 5YR 4/4 clearly evident throughout
7.5YR 4/4	Bt3	33-42	SiCL(SiL)	Mn Fe conc. common, sand is increasing, large areas of 7.5YR 7/1 where stripping has occurred is common
5YR 4/4	2BC1	42-62	L	Mn Fe conc. common, few small diameter (2-3mm) macropores, large areas of stripping, E-bodies, mixing zone between parent materials @ upper 4 inches
5YR 4/3	2BC2	62-70	L	Mn conc. common, large stripped areas still present, E- bodies, large increase in sand
5YR 4/6	2C1	70-81	SL(SCL)	7.5YR 7/3 stripped areas make-up a large portion of this horizon, sand increases sharply, Fe conc. common
(10R)2.5YR 4/6	3C2	81-116	SC	2.5YR 4/2 Fe depletions are common, Fe conc. common, stripped areas are common (5YR 5/3)
2.5YR4/8	3C3	116-131	SL(SCL)	Large stripped areas common, Fe conc. common, few Mn conc.
2.5YR 5/8	3C4	131-158^{+}	LS (SL)	

Transect 2 Test Hole

Parent material sequence is Loess over alluvium (2, 3). The 2nd lithologic discontinuity is marked by paleosol development at 81 inches. In this horizon, depletions are common indicating drainage impediment. Large areas of preferential flow begin at 33 inches and continue throughout the profile. These areas are marked stripped areas where coarser materials remain in the flow paths and the colors are significantly lighter. Drainage impediment at 81 inches may be caused by contrast in particle size with underlying horizon.

Described by: Kevin Raley
Date 6-6-02

EMI DATA

Method	**Day one (mS/m)**	**Day two (mS/m)**
Manual (EM31)		6.3
Mobile (EM 31)	6.7	7.7
Manual (EM 38)		12.5

Medium conductivity for transect (expected and observed)

	Horizon	Depth	Texture	Comments
(7.5)10YR 4/4	Ap	0-7	SiL	Roots and root channels common
7.5YR 4/6	Bt_1	7-19	SiCL	Few Mn and Fe conc., root channels common, clay films, (clear evidence of illuvaiation)
7.5YR 4/4	Bt_2	19-34	SiCL	Mn conc. common, clay increases slightly, few Fe conc., clay pockets/films clearly present
7.5YR 4/4	Bt_3	34-56	SiL(SiCL)	Clay films present but decreasing in amount, Mn conc., common, small and large stripped areas (7.5YR 7/1)
7.5YR 4/4	BC_1	56-69	SiL	Few large dia. Macropores (4mm), Mn conc. common, Fe conc. few, slight sand increase, stripped areas common but decreasing in number
5YR 4/4	$2BC_2$	69-85	L(CL)	Stripped areas common, horizon is pocketed with E bodies, significant increase in sand
2.5YR 4/6	$2BC_3$	85-93	CL	Fe, Mn conc. common, large stripped areas, 5YR 4/2 depletions are common, small diameter macropores (2mm) common
2.5YR 4/8	$2C_1$	93-105	SCL	Small stripped areas common, Mn Fe conc. common, heavy pick up in sand, large diameter macropores common (4mm)
2.5YR 3/6	$2C_2$	105-113	SCL	Large stripped areas common, clay increases dramatically, Mn conc. common, may be 2nd alluvial layer
2.5YR 5/6	$2C_3$	113-138	SC	Fe conc. common, horizon is dominated by large preferential flow, depletions(2.5YR 5/2) few, areas of clay films evidence of clay movement (paled) subsoil
2.5YR 4/6	$2C_4$	138-153	SCL	Fe Mn conc. common, 2.5 YR 5/2 depletions common, stripped areas common, small diameter macropores common
5Yr 4/6	$2C_5$	$153\text{-}162^+$	SL	Fe Mn conc. common

Transect 2-6

Loess extends to 69 inches. Possibly 3 separate Alluvial deposits under-lying the loess (85-105, 105-138, $138\text{-}162^+$). Each alluvial layer shows an increase in clay near the upper boundary and horizons adjacent to strongly contrasting particle size class show water movement restriction (85-93, 113-138). Unsure as to whether or not deeper tertiary material has been reached.
Described by: Kevin Raley
Date: 6-6-02
EMI DATA

Method	**Day one (mS/m)**	**Day two (mS/m)**
Manual (EM31)	7.7	7.5
Mobile (EM 31)	7.7	8.1
Manual (EM 38)	9.5	10.3

Highest conductivity for transect (expected and observed)

GPR Protocol

1) The geophysical team calibrates the GPR over an object of known depth. This calibration enables the team to reference the depth of GPR scans for the survey area. Soil samples are used to calibrate the equipment, but they are not as reliable as other methods.

2) The GPR is recalibrated on-site in accordance with the operating manual. The mobile GPR system allows for coverage of an entire field instead of a few selected transects. The GPR system is also linked to a differential global positioning system (DGPS) for positional accuracy. A handheld GPS unit is used for navigating the field and determining what areas are left unsurveyed.

3) The GPR scans are thoroughly examined in the lab for any anomalies or recognizable patterns. The examination of the GPR data also includes classification by a fuzzy neural network (F-NN) program specifically designed for such applications. The end product of the classification program is a map of similar properties within a field. Once relationships are established to soil properties in that field, it is essentially a type of soil map.

An all-terrain vehicle (ATV) pulls survey tools that were designed and built by Leonard (2001) to mobilize the geophysical equipment. A non-metallic cart is used as the towed field carrier for the EMI survey. The conductivity meter is placed far enough back from the ATV so electrical noise and metal parts do not affect the measurements. A non-metallic skid was also designed and built to house a single 200 MHz antenna for field

towing. These tools reduce the number of operators from two or more to one and significantly reduce time in the field.

System Modifications

The geophysical instruments are sensitive to temperature, moisture, and atmospheric conditions, which make finding an acceptable time to survey challenging. The occurrence of extreme hot or cold conditions can cause the internal tape drive on the GPR to drag or stop working completely. The ATV is retrofitted to decrease the occurrence of extreme temperatures that exceed the GPR manufacturer's recommended operating range of 0-35^{0}C. Temperatures routinely exceed the operating range of the GPR equipment during acceptable survey times, and data must be collected regardless of the conditions. The survey equipment is housed in a van box (fig. A.1) on the ATV, which serves as a protective shield from moisture and dust during field surveying. The box is insulated on the inside with a thin reflective material that has a high insulation resistance (R) value to keep the box cool in the summer and warm in the winter. Four holes are cut into the sides of the van box to allow for additional ventilation if needed.

Supplying power to the equipment during field data collection is also a problem. The traditional GPR survey uses two deep cycle marine batteries connected in parallel but provides power for a limited amount of time. The mobile GPR system employs a 120-VAC system for delivering power. An inverter supplies 1200-W of continuous power and 2400-W of peak power in two outlets. Connection to the power inverter is achieved using 00 gauge wire and LC-10 brass quick connectors. This allows the operator to easily hook up to the power supply of the ATV for the operation of survey equipment. As long as the

ATV is running, the battery remains charged, which provides an unlimited supply of power to the equipment. The inverter is protected from harsh field conditions by a polyvinyl chloride (PVC) box (fig. A.2). A 12-VDC fan circulates air inside the box. Vent holes in either side allow air in after it passes through vacuum cleaner filters. The box is sealed on three sides with weather stripping held in place by caulk.

A laptop computer contained within the van box records geographical location data from the GPS that is positioned directly above the GPR antenna (fig. A.3). The computer runs a program that places a marker into the GPR file at a set interval throughout the course of the survey. The program eliminates the use of survey flags, removing a step in the pre-survey stage of data collection. The operator can view the output of the GPR unit or laptop by using a keyboard/video/monitor (KVM) switch, which resides in the van box. The KVM switch allows the operator to control both computers with a standard PS/2 mini-keyboard and mouse. Hot keys on the keyboard allow for easy switching between user interfaces on the laptop and GPR equipment. A single monitor is positioned so that the operator can view it at any time during data collection. A mounting bracket (fig. A.4) and protective box (fig. A.5) were designed and built so the operator could easily check the progress of data collection while continuing to drive the ATV. Figure A.6 represents an overview of the entire survey setup including equipment housed in the van box and on the ATV.

The extremely large amounts of data that are gathered by the GPR in a single day would take many hours for researchers to manually process and interpret. The errors associated with manual processing and interpretation of radargrams are often the limiting

factors in successfully surveying large areas with GPR. On-going research in pattern recognition software by Odhiambo *et al*. (2002) shows promise for quickly and accurately classifying soil profiles captured through GPR imagery. The unsupervised neural network (NN) classification of GPR data will only be based on data from a single file. As we build a database of GPR scans, a supervised NN will be able to classify data based on information and patterns that occur in previous scans. There is also a possibility to incorporate this classification method in real time for precision agriculture applications.

References

Leonard, L.L. 2001. Mobile field systems for rapid subsurface data acquisition using electromagnetic induction and ground penetrating radar. Master's Thesis, University Of Tennessee.

Odhiambo, L.O., R.S. Freeland, R.E. Yoder, and J.W. Hines. 2002. Application of fuzzy-neural network in classification of soils using ground-penetrating radar imagery. ASAE paper No. 023097. St. Joseph, MI: ASAE.

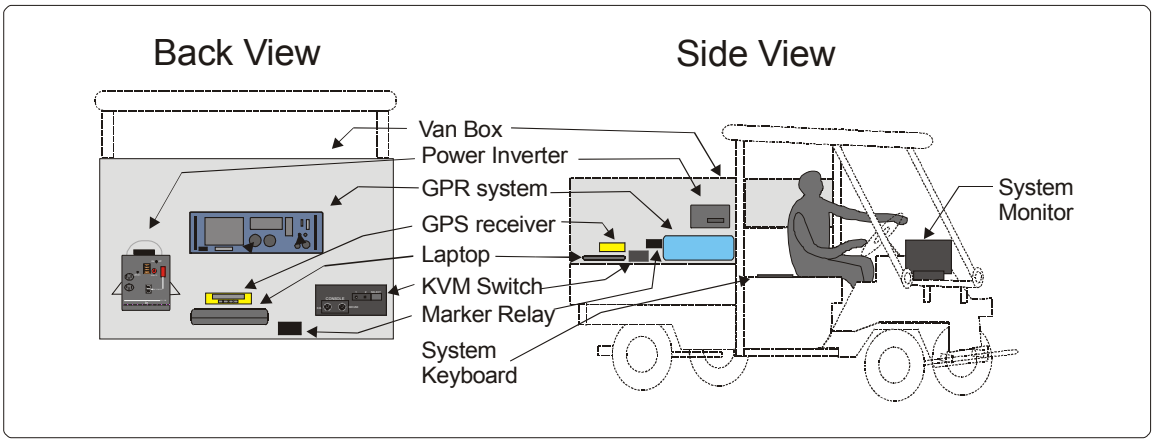

Figure A.1-- Mobile survey setup

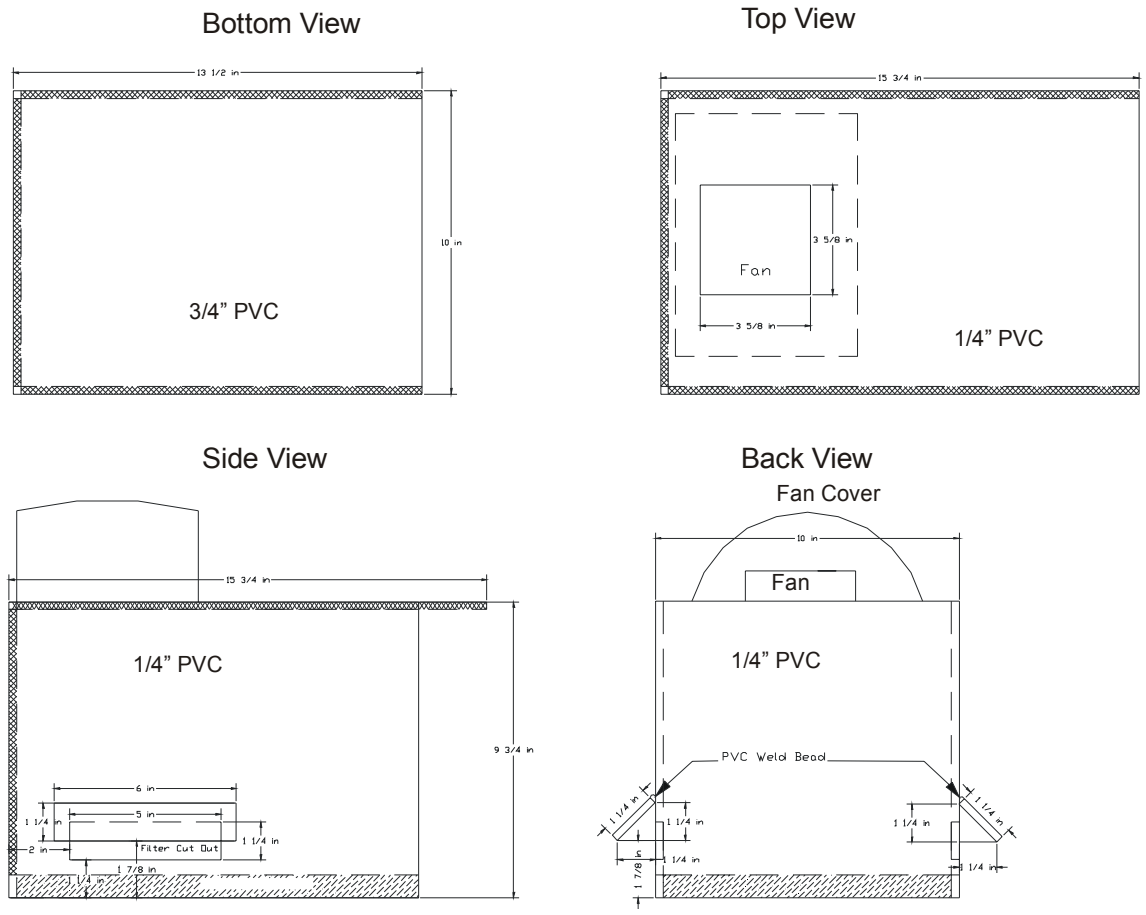

Figure A.2-- Inverter box design

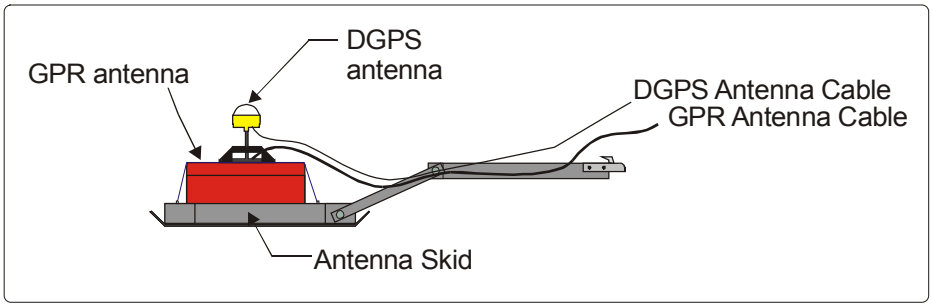

Figure A.3-- Mobile GPR components

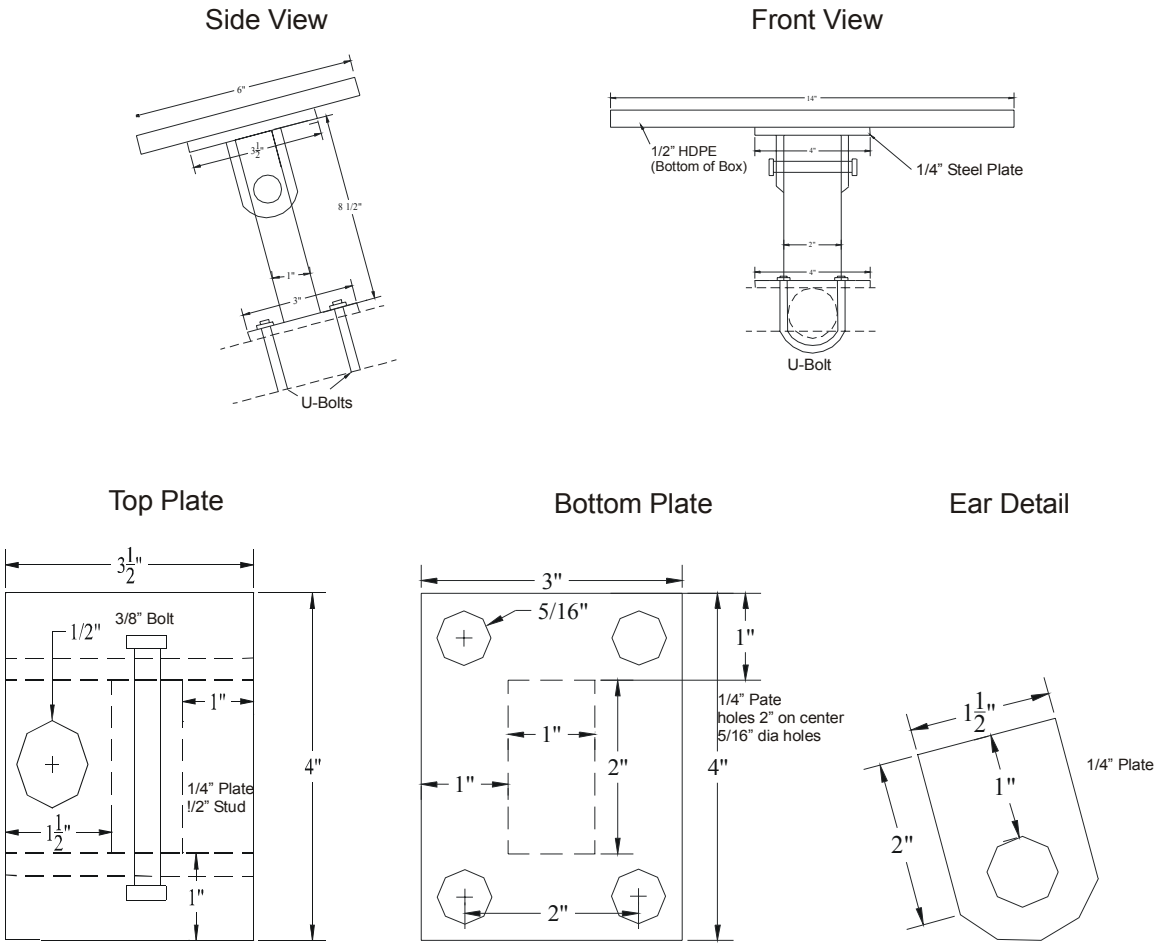

Figure A.4-- Mounting bracket for system monitor box

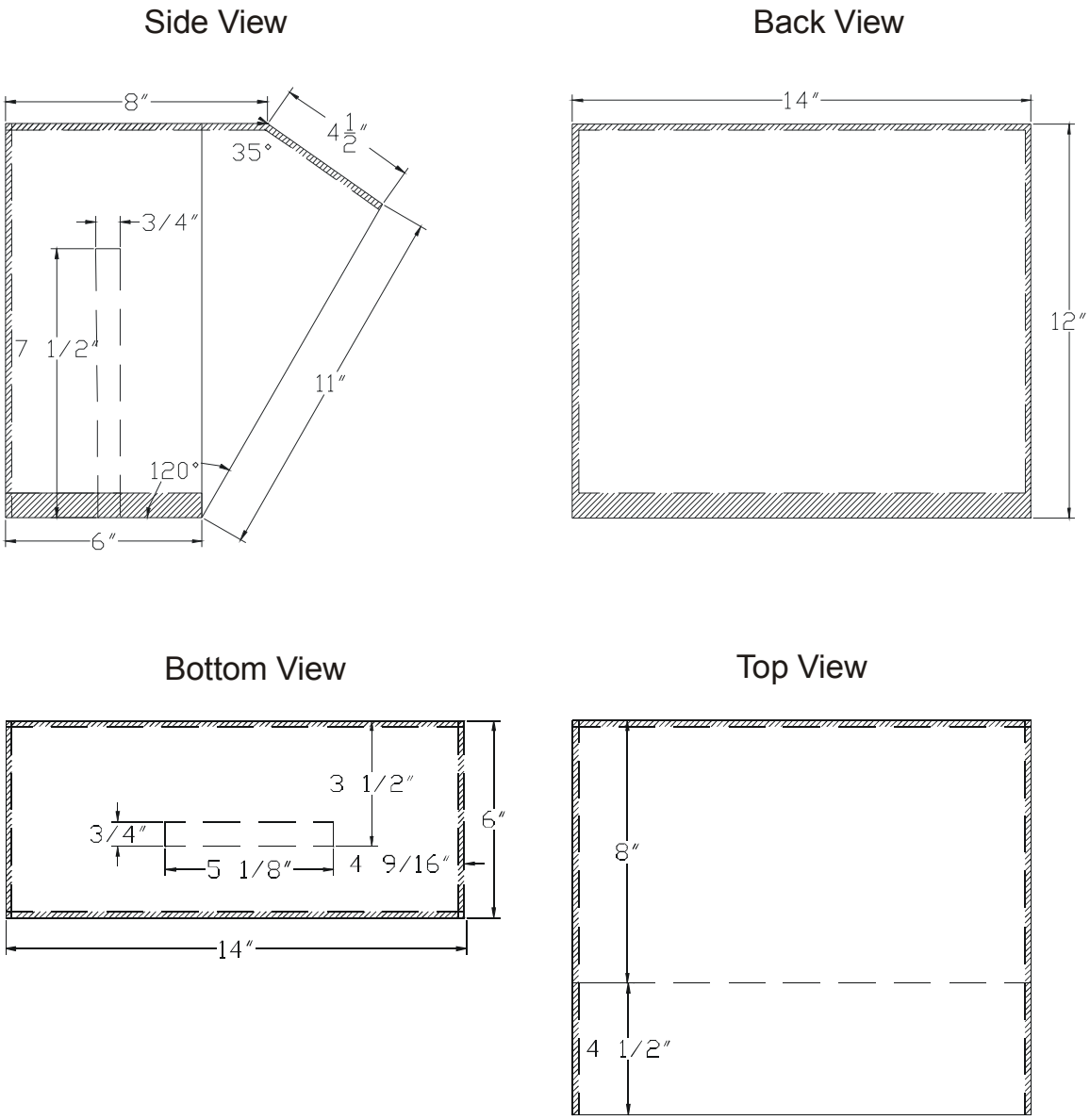

Figure A.5-- System monitor box design

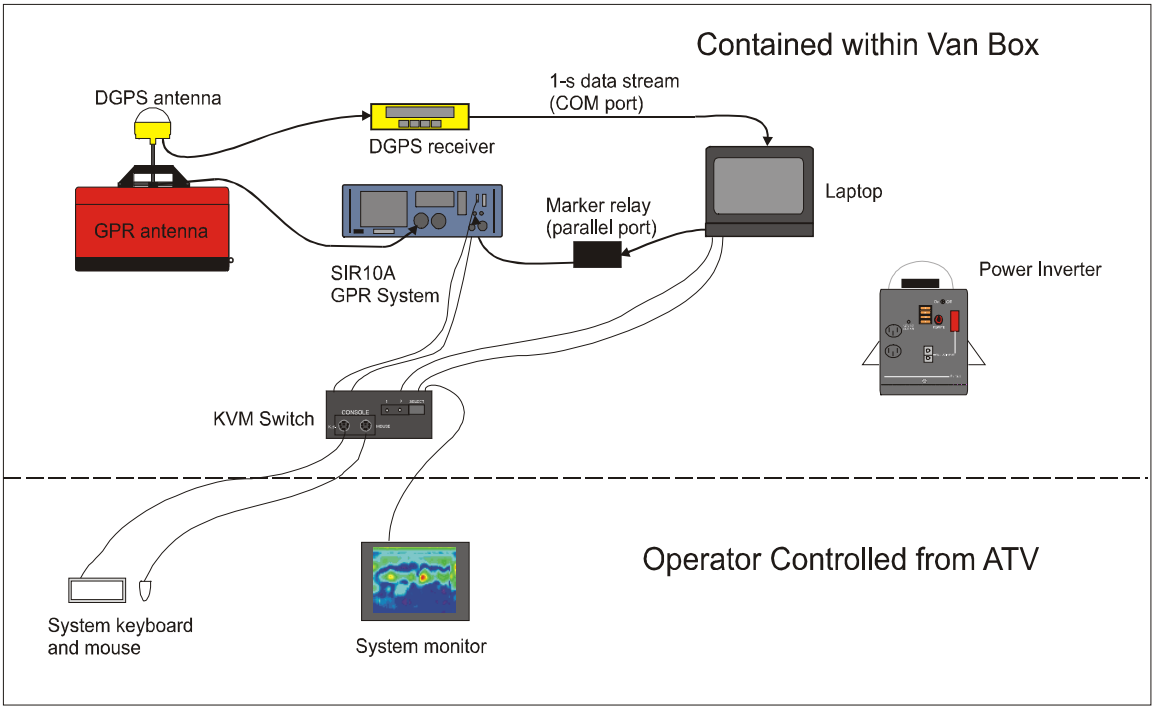

Figure A.6-- Survey schematic

Vita

Robert Claborne Wilson was born on March 9, 1978 in Crossville, Tennessee. He attended Cumberland County High School, and graduated in May 1996. In August 1996 he entered Roane State Community College and earned an Associate of Science degree in May 1998. In August 1998 he transferred to Tennessee Technological University and earned a Bachelors of Science degree in Agriculture with a concentration in Environmental Agriscience in May 2000. He began his work towards a Masters of Science degree in Biosystems Engineering Technology in June 2000, and was employed as a graduate research assistant. In October 2001 he was employed by the Biosystems Engineering and Environmental Science Department as a full-time research associate. After graduation in August 2003 he will go to work with TVA as a photointerpretation analyst.